Korea-Australia Rheology Journal, 31(4), 211-228 (November 2019) www.springer.com/13367
DOI: 10.1007/s13367-019-0022-5

Stability of flows with the BMP model in the yield stress limit

Ian Frigaard[1,*] and Alondra Renteria[2]
[1]*Departments of Mathematics and Mechanical Engineering, University of British Columbia, Vancouver V6T 1Z2, Canada*
[2]*Department of Mechanical Engineering, University of British Columbia, Vancouver V6T 1Z4, Canada*

(Received July 7, 2019; final revision received September 8, 2019; accepted September 16, 2019)

Common features of complex fluids include yield stress, thixotropy and elasticity. A comprehensive constitutive model attempts to effectively predict flow responses dominated by such characteristics. Nevertheless, when constructing a constitutive model that deals with yield stress fluids one must try to preserve the fundamental characteristics of a yield stress. This paper explores the static and energy stability of a classic viscoplastic model when elasticity or thixotropy are introduced. We exemplify this analysis using the Bautista-Manero-Puig (BMP) model in the yield stress limit. This model has the advantages of a small number of parameters, a physically intuitive kinetic equation, and it has been widely used to represent fluids with time-dependent rheology. We analyze stability of the BMP model for different limiting cases. Viscoplastic flows (VP), where we remove the elasticity and thixotropy behaviour, are shown to respond qualitatively in an analogous way to a simple yield stress fluid, *e.g.* Bingham, Casson. Thixo-visco-plastic flows (TVP), identified by having an elastic time scale much faster than the thixotropic and viscous timescales, preserve the notion of static and energy stability but with bounds now dependent on the stress and no longer with finite time decay. Finally, elasto-visco-plastic flows (EVP), where the thixotropic evolution is faster than the elastic, have a static stability limit perturbed linearly by the Weissenberg number. Numerically solved examples of each of flow regime are given for stopping and starting flow, based on the plane Poiseuille flow.

Keywords: viscoelastoplasticity, thixotropy, yield stress fluids, energy stability, BMP model

1. Introduction

The BMP model (Bautista *et al.*, 1999), is a visco-elastic extension of a thixotropic generalized Newtonian fluid model proposed by Fredrickson (1970). The model is popular due to its flexibility and intuitive simplicity. This interest and recognized limitations, have led to a range of modifications and extensions, some of which we review later. However, the focus of this paper is a particular limiting case of the BMP model, in which true yield stress behaviour is purported to occur.

Simple (or ideal) yield stress fluids, such as the Bingham, Herschel-Bulkley and Casson fluids, have widespread practical application and are extensively studied for both applications and fundamental aspects; Frigaard (2019a). However, it has long been known that these models are limited in describing the full range of rheological behaviours observed as reviewed by Balmforth *et al.* (2014), Bonn *et al.* (2017). There is a consequent current trend to extend these models in ways that can describe a wider range of observed flow phenomena. Elasticity featured in some of the earliest descriptions of viscoplastic fluids, *e.g.*, Schwedoff (1900), Oldroyd (1947), which are amongst the first elasto-visco-plastic (EVP) fluids. More recently Saramito (2007; 2009) has developed these ideas into a modern tensorial context. The Saramito model has had good success for example in explaining the fore-aft asymmetry of a sphere moving slowly in Carbopol gel, as observed by Putz *et al.* (2008), Holenberg *et al.* (2012). This and other models are compared computationally by Fraggedakis *et al.* (2016).

Thixotropic models have a long history; see *e.g.*, the reviews of Mujumdar *et al.* (2002), Mewis and Wagner (2009). In the yield stress context, structural changes with time are natural in applications and these concepts applied simplistically, have been in use industrially since the 1960's, *e.g.,* the gel strength of a drilling fluid and more recently the development of waxy phases in heavy crude oils. Thixotropy has also been used as a tool to explain transient aspects of the yield stress, as in *e.g.*, the toy model of Coussot and Bonn (Coussot *et al.*, 2002; Moller *et al.*, 2009), or models discussed by de Souza Mendes and Thompson (2012). These thixo-visco-plastic (TVP) fluid developments are reviewed by de Souza Mendes and Thompson (2019).

Finally, there are models recently proposed which combine thixotropy and elasticity in modelling viscoplastic flows (TEVP fluid models), such as those of de Souza

This paper is based on an invited lecture presented by the corresponding author at the 30th Anniversary Symposium of the Korean Society of Rheology (The 18th International Symposium on Applied Rheology (ISAR)), held on May 21-24, 2019, Seoul.
*Corresponding author; E-mail: E-mail: frigaard@math.ubc.ca

Mendes *et al.* (2018), or Dimitriou and McKinley (2019). An interesting physical perspective is also given by Ewoldt and McKinley (2017). While it is of interest to introduce new rheological models to capture different phenomena, we should also take the opportunity to re-examine existing TEVP models, such as the BMP model, which is conceptually simple and does not have a zoo of parameters, to see how they perform.

This is the intent here, where we look at the limit of the BMP model with zero low shear fluidity. While we expect some benefits from using a more complex rheological model, we should not destroy essential features of simpler models that we regard as representative. Simple yield stress fluids share many qualitative features of other generalized Newtonian fluids, *e.g.*, shear-thinning, but also have unique behaviours. In yield stress fluid flows, parts of the region are occupied by yielded fluid and other parts by unyielded fluid. The latter are termed "plugs", have zero strain rate (*i.e.*, move in rigid motion) and may be further classed as moving or static plugs, with the latter arising in regions attached to a wall.

Other unique features of simple yield stress fluids centre on flow stability. Purely viscous fluids are unable to resist a shear stress while at rest. Shear stresses comes from either imposed body forces or applied surface tractions, *e.g.*, flow along a pipe under the action of a pressure drop. In contrast yield stress fluids may resist this forcing of the flow, *i.e.*, a static flow is possible where a purely viscous fluid would flow. This static stability is characterized by exceeding a critical yield number, representing a critical ratio of the yield stress to the driving stresses of the flow, *i.e.*, the pipe does not flow, the paint stays on the wall, *etc.*

A further interesting feature concerns the energy stability of these static states. In other words, what happens to the kinetic energy of a perturbation from the base state? First, as with other purely viscous generalized Newtonian fluids for interior flows the velocities remain bounded since the viscous part of the dissipation becomes dominant with respect to the work driving the flow. At smaller velocities however, provided the critical yield number is exceeded, the plastic dissipation exceeds the work driving the flow. This results in energy stable flows, typically globally so, and in many cases we have decay of the solution to zero in finite time; see *e.g.*, Karimfazli and Frigaard (2016). This feature allows the yield stress to be used as control parameter in different situations.

An outline of the paper is as follows: in section 2 we introduce the BMP model and the governing scaled equations for the class of flows we analyze. In section 3, we take the visco-plastic limit ($W = \Lambda = 0$) of the BMP model and develop static stability and energy stability results that are analogous to those for the classic Bingham model. Simple examples are given using steady and unsteady plane Poiseuille flows. In section 4, we explore analogous stability bounds for thixo-visco-plastic ($W = 0,\ \Lambda \neq 0$) flows when activating the structural timescale in the inelastic BMP model. Later, in section 5 we examine the stability bounds for the elasto-visco-plastic (EVP) flows, where we conversely neglect thixotropy and retain elasticity ($\Lambda = 0,\ W \neq 0$). Finally, in section 6 we discuss and reflect on the implications that these elastic and thixotropic elements have in a constitutive model that aims to preserve features of yield stress behaviour.

2. The BMP model

Our study concerns incompressible flows of fluids governed by the BMP model, in either ducts or interior domains. These flows are governed by momentum and mass conservation equations:

$$\hat{\rho}\frac{\hat{D}}{\hat{D}\hat{t}}\hat{\mathbf{u}} = -\hat{\nabla}\hat{p} + \hat{\nabla}\cdot\hat{\underline{\underline{\boldsymbol{\tau}}}} + \hat{\mathbf{f}}, \tag{1}$$

$$\hat{\nabla}\cdot\hat{\mathbf{u}} = 0 \tag{2}$$

where $\hat{\rho}$, $\hat{\mathbf{u}}$, $\hat{p}$, $\hat{\underline{\underline{\boldsymbol{\tau}}}}$, and $\hat{\mathbf{f}}$ are respectively, the density, velocity, pressure, total stress, and a body force. We denote dimensional quantities with the $\hat{}$ symbol for clarity; $\frac{\hat{D}}{\hat{D}\hat{t}}$ is the usual material derivative. The total stress follows a UCM approach:

$$\hat{\underline{\underline{\boldsymbol{\tau}}}} + \frac{1}{\hat{G}_0\hat{\varphi}}\overset{\nabla}{\hat{\underline{\underline{\boldsymbol{\tau}}}}} = \frac{1}{\hat{\varphi}}\hat{\underline{\underline{\dot{\boldsymbol{\gamma}}}}}. \tag{3}$$

Here $\overset{\nabla}{}$ denotes the usual upper convected derivative, $\hat{G}_0$ is the stress modulus, $\hat{\varphi}$ is the fluidity, and $\hat{\underline{\underline{\dot{\boldsymbol{\gamma}}}}}$ the strain rate tensor:

$$\hat{\dot{\gamma}}_{ij} = \frac{\partial\hat{u}_i}{\partial\hat{x}_j} + \frac{\partial\hat{u}_j}{\partial\hat{x}_i}. \tag{4}$$

The fluidity evolves according to:

$$\frac{\hat{D}\hat{\varphi}}{\hat{D}\hat{t}} = \frac{1}{\hat{\lambda}}(\hat{\varphi}_0 - \hat{\varphi}) + \hat{K}_0(\hat{\varphi}_\infty - \hat{\varphi})\ \hat{\underline{\underline{\boldsymbol{\tau}}}}:\hat{\underline{\underline{\dot{\boldsymbol{\gamma}}}}}, \tag{5}$$

with $\underline{\underline{\mathbf{a}}}:\underline{\underline{\mathbf{b}}} = \frac{1}{2}a_{ij}b_{ij}\left(\equiv\frac{1}{2}\Sigma_{ij}a_{ij}b_{ij}\right)$, *i.e.*, summation is implicit. Note we use the above inner product for tensors, denote components by their indices with no bold script and the associated tensor norm is denoted $a = \sqrt{\underline{\underline{\mathbf{a}}}:\underline{\underline{\mathbf{a}}}}$.

The Fredickson equation, Eq. (5) is written in terms of the fluidity $\hat{\varphi}$, which is the inverse of the viscosity. This kinetic equation describes the evolution of structure due to two contributions: the buildup of structure with a Maxwell-like characteristic time $\hat{\lambda}$, and the breakdown of structure by irreversible work, proportional to the dissipation rate $\hat{\underline{\underline{\boldsymbol{\tau}}}}:\hat{\underline{\underline{\dot{\boldsymbol{\gamma}}}}}$ and a rate constant $\hat{K}_0$. Assuming positivity of the dissipation term, the fluidity is bounded by two

Newtonian plateaux: $\hat{\varphi}_0 < \hat{\varphi}_\infty$, representing low and high shear limits respectively. Our specific interest in this paper is the yield stress limit of this model, which occurs if $\hat{\varphi}_0 = 0$. We assume this throughout the paper.

The above is the original model from Bautista *et al.* (1999). For variants/extensions $\hat{\underline{\underline{\boldsymbol{\tau}}}}$ can be split into elastic and solvent components, in what is called the MBM (modified Manero-Bautista) model; see Manero *et al.* (2002), Boek *et al.* (2005). Alternatively, it may be split into particle and solvent components if a suspension is considered, *e.g.*, Calderas *et al.* (2013). Relaxing the requirement that $\hat{K}_0$ be constant and introducing strain rate dependency is associated with shear-banding variants of the model, *e.g.*, as in Bautista *et al.* (2007).

2.1. Scaled flows

Later we shall use the plane Poiseuille flow configuration to illustrate our results. However, we wish to consider flows in more generality and in particular the concept of a critical yield number that divides flowing states from static states. This does not apply to fluids for which $\hat{\varphi}_0 > 0$, which can show only very viscous behaviour.

Therefore, we consider a domain Ω characterised by a length-scale $\hat{H}$ and suppose that the driving force of the flow has a characteristic stress scale $\hat{\tau}_0$. As an example, in a duct flow we might expect a pressure drop $\Delta\hat{P}$ along a length $\hat{L}$ and using $\hat{H}$ as representative transverse length (*e.g.*, radius, channel half-width, etc.), we might have:

$$\hat{\tau}_0 = \frac{\Delta\hat{P}}{\hat{L}}\hat{H}\,. \tag{6}$$

Alternatively, consider an interior domain where the body force $\hat{\mathbf{f}}$ drives the flow. Here we assume a Helmholtz decomposition: $\hat{\mathbf{f}} = -\hat{\nabla}\hat{\phi} + \hat{\nabla}\times\hat{\mathbf{A}}$, denoting the irrotational and divergence free components, respectively. The irrotational part (*e.g.*, gravity) simply modifies the pressure and does not drive the flow. Thus here we would take:

$$\hat{\tau}_0 = \hat{H}\left\|\hat{\nabla}\times\hat{\mathbf{A}}\right\|, \tag{7}$$

with $\|\cdot\|$ some suitable norm. In more complex flows the driving force could be buoyancy, *e.g.*, from thermal expansion, or could arise from electro-magnetic effects, although these cases also involve further field equations.

To normalize our equations we scale lengths with $\hat{H}$, all stresses with $\hat{\tau}_0$, velocity with $\hat{U}_0 = \hat{\tau}_0\,\hat{\varphi}_\infty\,\hat{H}$, time with $\hat{H}/\hat{U}_0$, and the fluidity with $\hat{\varphi}_\infty$. This results in the following dimensionless system, that we study for the remainder of the paper.

$$Re\frac{D\mathbf{u}}{Dt} = -\nabla p + \nabla\cdot\underline{\underline{\boldsymbol{\tau}}} + \mathbf{f}\,, \tag{8}$$

$$0 = \nabla\cdot\mathbf{u}\,, \tag{9}$$

$$W\overset{\nabla}{\underline{\underline{\boldsymbol{\tau}}}} = \underline{\underline{\dot{\boldsymbol{\gamma}}}} - \varphi\underline{\underline{\boldsymbol{\tau}}}, \tag{10}$$

$$\Lambda\frac{D\varphi}{Dt} = -\varphi + (1-\varphi)\frac{\underline{\underline{\boldsymbol{\tau}}}:\underline{\underline{\dot{\boldsymbol{\gamma}}}}}{Y^2} \tag{11}$$

The 4 dimensionless groups here are the Reynolds number (*Re*), Weissenberg number (*W*), the thixoviscous number (Λ), and the yield number (*Y*). The first 3 of these are defined as in Castillo and Wilson (2018):

$$Re = \frac{\hat{\rho}\hat{U}_0^2}{\hat{\tau}_0} = \frac{\hat{U}_0}{\hat{H}}\hat{\rho}\hat{\varphi}_\infty\hat{H}^2,\; W = \frac{\hat{U}_0}{\hat{G}_0\hat{\varphi}_\infty\hat{H}},\; \Lambda = \hat{\lambda}\frac{\hat{U}_0}{\hat{H}}\,. \tag{12}$$

We see that *Re* is the ratio of the viscous timescale ($\hat{\rho}\hat{\varphi}_\infty\hat{H}^2$) to the flow timescale ($\hat{H}/\hat{U}_0$). Similarly *W* compares the viscoelastic relaxation time ($[\hat{G}_0\hat{\varphi}_\infty]^{-1}$) to the flow timescale and Λ compares the buildup timescale to the flow timescale. For vanishing *Re* we recover Stokes flows, vanishing *W* leads to thixo-visco-plastic (TVP) flows and vanishing Λ leads to elasto-visco-plastic (EVP) flows.

Below we study the different limits of these flows in which one or both of *W* and Λ is set to zero. In doing this our physical interpretation of these limits is dynamic, as discussed nicely in Castillo and Wilson (2018), *i.e.*, $W = 0$ means simply that the elastic timescale is much faster than the structural and viscous timescales.

The remaining dimensionless group is the yield number *Y*:

$$Y = \sqrt{\frac{\hat{H}}{\hat{\tau}_0\hat{K}_0\hat{\lambda}\hat{U}_0}} = \frac{1}{\hat{\tau}_0\sqrt{\hat{\lambda}\hat{K}_0\hat{\varphi}_\infty}} \tag{13}$$

which plays the role of a dimensionless yield stress below. In the BMP model there is critical stress $\hat{\tau}_c$ which is identified as the stress value that separates primary creep from accelerating flow (under constant imposed shear stress); see Fredrickson (1970). This is identified as

$$\hat{\tau}_c = \frac{1}{\sqrt{\hat{\lambda}\hat{K}_0\hat{\varphi}_\infty(1-2\hat{\varphi}_0/\hat{\varphi}_\infty)}} \to \frac{1}{\sqrt{\hat{\lambda}\hat{K}_0\hat{\varphi}_\infty}}\,, \tag{14}$$

as $\hat{\varphi}_0 \to 0$. Thus *Y* is the ratio of $\hat{\tau}_c$ and the imposed stress scale $\hat{\tau}_0$. This is the usual interpretation of a yield number, provided that we accept $\hat{\tau}_c$ as a yield stress.

Equation (11) is a kinetic equation for φ. A steady state of this equation implies a balance between the kinetics of structural build-up and destruction, *i.e.*, that there is an equilibrium constant that captures the ratio of the rate constants for the two kinetic processes: $\hat{\lambda}^{-1}$ and $\hat{\tau}^2\hat{K}_0\hat{\varphi}_\infty$, respectively. The parameter Y^2 is thus a measure of the equilibrium constant (growth rate/destruction rate), evaluated at the imposed stress of the system $\hat{\tau}_0$. Thus later, as we conside $\Lambda = 0$ for non-zero *Y*, *Re*, and *W*, this just means that the timescale for structural build-up is fast, relative to viscous and elastic timescales, but there is still a rate equilibrium balance between build-up and destruction processes.

3. Visco-plastic flows: $W = \Lambda = 0$

We first look at the visco-plastic flow (VP) limit of the BMP model in which $W = \Lambda = 0$. Equation (10) implies that

$$\dot{\underline{\underline{\gamma}}} = \varphi \underline{\underline{\tau}}, \tag{15}$$

from which we see the stress is inelastic and that $\underline{\underline{\tau}} : \dot{\underline{\underline{\gamma}}} \geq 0$. Provided $\underline{\underline{\tau}}$ is finite, as expected, we see that the strain rate vanishes as $\varphi \to 0$. On the other hand, assuming that $\dot{\gamma}$ and φ vanish at the same rate it is possible to have non-zero stress as $\dot{\gamma} \to 0$. Turning to the kinetic equation, we have steady fluidity, $\varphi = \varphi_s$:

$$0 = -\varphi_s + (1-\varphi_s)\frac{\underline{\underline{\tau}} : \dot{\underline{\underline{\gamma}}}}{Y^2}, \tag{16}$$

where by virtue of Eq. (15), $\underline{\underline{\tau}} : \dot{\underline{\underline{\gamma}}} = \tau^2 \varphi = \tau \dot{\gamma} = \dot{\gamma}^2/\varphi$, where we have written $\tau = \sqrt{\underline{\underline{\tau}} : \underline{\underline{\tau}}}$ and $\dot{\gamma} = \sqrt{\dot{\underline{\underline{\gamma}}} : \dot{\underline{\underline{\gamma}}}}$.

In other words, φ is interpreted as having evolved rapidly to φ_s which is slaved to the stress (or the strain rate, or the dissipation rate). Using the stress we may write:

$$0 = \varphi_s \left[(1-\varphi_s)\frac{\tau^2}{Y^2} - 1 \right]. \tag{17}$$

Provided $\tau \leq Y$, the only solution of this equation is $\varphi_s = 0$. For $\tau > Y$, there are 2 solutions: $\varphi_s = 0$ and $\varphi_s = 1-(Y/\tau)^2$. The latter of these is the stable branch for the kinetic equation. If the stress ($\tau > Y$) was held constant, then $\varphi(t) = 0$ would be unstable for small $\Lambda > 0$, resulting in $\varphi(t) \to 1-(Y/\tau)^2 = \varphi_s$.

We may express φ_s in various ways, for convenience:

$$\varphi_s(\tau/Y) = \begin{cases} 0, & \tau/Y \leq 1, \\ 1-(Y/\tau)^2 & \tau/Y > 1, \end{cases} \tag{18}$$

$$\varphi_s(\tau\dot{\gamma}/Y^2) = \frac{(\tau\dot{\gamma}/Y^2)}{1+(\tau\dot{\gamma}/Y^2)}, \tag{19}$$

$$\varphi_s(\dot{\gamma}/Y) = -\frac{(\dot{\gamma}/Y)^2}{2} + \sqrt{-\frac{(\dot{\gamma}/Y)^4}{4} + (\dot{\gamma}/Y)^2}. \tag{20}$$

3.1. BMP and Bingham models

As discussed above, if $\varphi_s = 0$ then $\dot{\gamma} = 0$. Assuming the stable branch, we see that $\tau \leq Y \Leftrightarrow \varphi_s = 0 \Leftrightarrow \dot{\gamma} = 0$, and from this perspective, Y "is as good a yield stress as the Bingham one" as stated by Bautista *et al.* (1999). Indeed, we may compare the BMP and Bingham models directly for any steady flow in this limit.

For example, for a plane Poiseuille flow with the scaling adopted we would solve:

$$0 = 1 + \frac{d}{dy}\tau_{xy},\ y \in [-1, 1], \quad \Rightarrow \tau_{xy} = -y. \tag{21}$$

The region $|y| \leq Y$ is a plug for both fluids: $U'(y) = 0$. In the yielded regions ($|y| > Y$) we have for the Bingham fluid: $|U'(y)| = |y| - Y$ and for the BMP model, $|y| = \tau = \dot{\gamma}/\varphi_s$, leading to: $|U'(y)| = |y| - Y^2/|y|$. In both cases we may integrate to find the velocity $U(y)$. Thus, for the same pressure gradient and associated scaling the yield surfaces are identical, the velocity gradient vanishes at the yield surface and the second derivative is discontinuous. However, the BMP model is less dissipative and this leads to significant differences in the velocity profile and mean velocity (effectively flow rate) as Y is varied, as illustrated in Fig. 1.

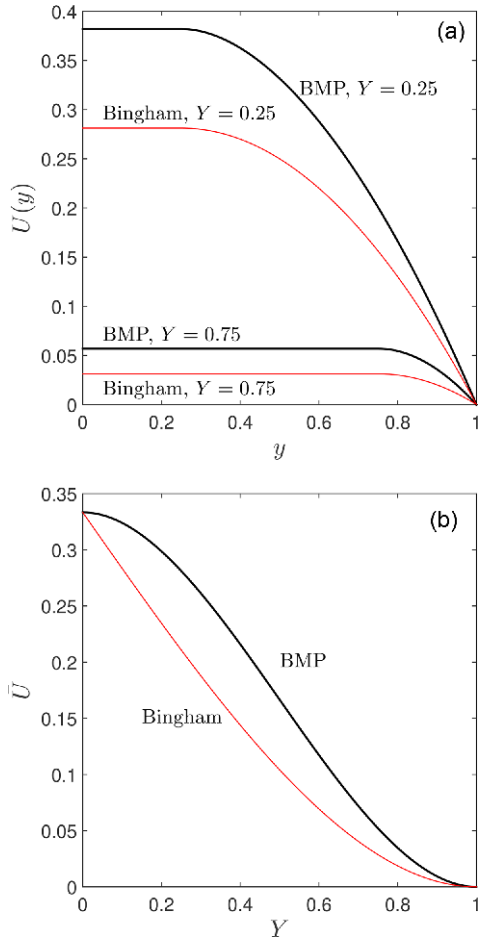

Fig. 1. (Color online) Comparison of the BMP and Bingham models for plane Poiseuille flow. (a) Velocity profile in half channel for several yield numbers. (b) Mean velocity vs yield number from (a).

3.2. Critical Y

We now address another aspect of a simple yield stress fluid, which is the defining feature of its dynamics: the critical yield number. Briefly, for a given flow there is a critical Y_c such that if $Y \geq Y_c$ then the velocity is $\mathbf{u} = 0$, *i.e.*, under imposed forcing for sufficiently large yield stress the flow will be static. This feature is evident in the above Poiseuille flow example, where simply taking $Y \geq Y_c = 1$

results in $U(y) = 0$.

For a more general steady flow we formulate the mechanical energy balance from the momentum equation by taking the dot product with $\mathbf{u}$ and integrating over Ω. The inertial contribution vanishes if either $\mathbf{u} = 0$ on the walls $\partial\Omega$ (*e.g.*, interior flow driven by $\mathbf{f}$), or if the net flux of kinetic energy into Ω is zero (*e.g.*, common in a steady duct flow), or some combination of these. This results in:

$$0 = L(\mathbf{u}) - \langle \underline{\underline{\boldsymbol{\tau}}} : \underline{\underline{\dot{\boldsymbol{\gamma}}}}(\mathrm{u}) \rangle = L(\mathbf{u}) - \langle \tau\dot{\gamma}(\mathbf{u}) \rangle , \tag{22}$$

where $\langle \cdot \rangle$ denotes the integral over Ω and where $L(\mathbf{u})$ gives the net work input from the different driving mechanisms of the flow. Let us suppose that $\partial\Omega = \partial\Omega_v \cup \partial\Omega_s$, with $\mathbf{u} = 0$ on $\partial\Omega_w$ and the traction specified on $\partial\Omega_s$ (inflow and outflow boundaries). Then we have:

$$L(\mathbf{u}) = \langle \mathbf{u} \cdot \nabla \times \mathbf{A} \rangle + \int_{\partial\Omega_s} u_i[-(\phi + p)\delta_{ij} + \tau_{ij}]n_j ds , \tag{23}$$

where $\boldsymbol{\delta}$ is the Kronecker delta and $\mathbf{n}$ the outward normal on $\partial\Omega_s$. Specific examples are as follows.

Example 1: Interior flow

Here $\partial\Omega = \partial\Omega_v$ and $\partial\Omega_s = \varnothing$, so that $L(\mathbf{u}) = \langle \mathbf{u} \cdot \nabla \times \mathbf{A} \rangle = -\langle \mathbf{A} \cdot (\nabla \times \mathbf{u}) \rangle$, on using common vector identities and the divergence theorem. Here energy is generated by alignment of $\mathbf{A}$ with the vorticity, $(\nabla \times \mathbf{u})$.

Example 2: Fully developed duct flow

Here typically $\mathbf{A} = 0$, the irrotational component ϕ (*e.g.*, gravity) is incorporated into the modified pressure and the tractions are given at inflow and outflow in the form of an imposed pressure drop. With a uniform duct of dimensionless length l in direction x_1 (unit vector $\mathbf{e}_1$), the modified pressure difference imposed in our scaled system is equal to l and hence:

$$L(\mathbf{u}) = l \int_X u_1 dx_2 dx_3 = \langle \mathbf{u} \cdot \mathbf{e}_1 \rangle . \tag{24}$$

where X denotes the duct cross-section.

In both above examples, we see that $L(\mathbf{u})$ is a linear operator involving the dot product with a specified vector field, which is of order 1 in magnitude, due to the scaling. For the visco-plastic dissipation term in (22) we can write:

$$\langle \tau\dot{\gamma}(\mathbf{u}) \rangle = \langle \dot{\gamma}^2 / \varphi_s(\dot{\gamma}/Y) \rangle , \tag{25}$$

and from analyzing (20) we see that:

$$\varphi_s \sim \dot{\gamma}/Y - \dot{\gamma}^2/(2Y^2) \text{ as } \dot{\gamma} \to 0 ,$$
$$\varphi_s \sim 1 - (Y/\dot{\gamma})^2 \text{ as } \dot{\gamma} \to \infty , \tag{26}$$

which means that the dissipation term behaves qualitatively as a Bingham (or Cassson) fluid in the 2 limits. We can subtract the plastic dissipation term: $\langle \tau\dot{\gamma} \rangle = Y\langle \dot{\gamma} \rangle +$ $\langle (\tau - Y)\dot{\gamma} \rangle$, and the last term, which represents the viscous dissipation is positive, bounded below by $\sim \langle 0.5\dot{\gamma}^2 \rangle$ for all $\dot{\gamma}$, and asymptotes to $\sim \langle \dot{\gamma} \rangle^2$ from below, for large $\dot{\gamma}$; see Fig. 2.

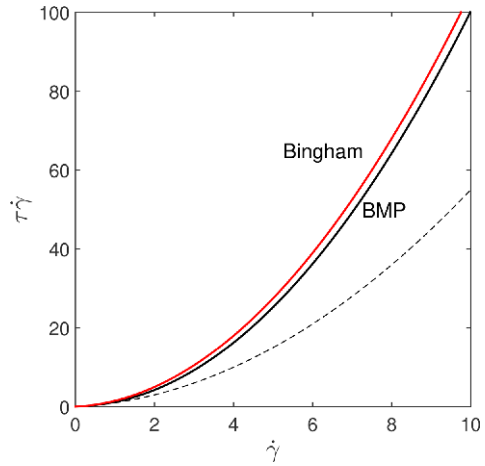

Fig. 2. (Color online) Dissipation of the BMP and Bingham models at $Y = 0.5$. The broken line denotes the lower bound: $Y\dot{\gamma} + 0.5\dot{\gamma}^2$.

Analysis now proceeds identically to the case of a Bingham fluid (or any other simple yield stress fluid). Assuming that $\mathbf{u} \neq 0$,

$$0 \leq \langle (\tau - Y)\dot{\gamma}(\mathbf{u}) \rangle = \langle \dot{\gamma}(\mathbf{u}) \rangle \left(Y - \frac{L(\mathbf{u})}{\langle \dot{\gamma}(\mathbf{u}) \rangle} \right) ,$$
$$\leq \langle \dot{\gamma}(\mathbf{u}) \rangle (Y - Y_c) , \tag{27}$$

$$Y_c = \sup_{\mathbf{v} \neq 0, \mathbf{v} \in \mathcal{V}} \left\{ \frac{L(\mathbf{v})}{\langle \dot{\gamma}(\mathbf{v}) \rangle} \right\} . \tag{28}$$

This definition of Y_c is identical to that for a Bingham fluid under the same flow conditions and the function space $\mathcal{V}$ of the solution is also identical. From Eq. (27) we see that $Y \geq Y_c$ ensures that $\mathbf{u} = 0$.

A number of theoretical results could now be proven regarding existence and uniqueness of steady solutions, continuity of the solutions with respect to forcing and Y, convergence as $Y \to Y_c$, velocity minimization and stress maximization principles (for non-inertial flows). These use standard methods from convex analysis and variational inequalities. There appears to be no qualitative difference to the same results for a Bingham fluid, but some work would need to be done to develop these rigorously. Examples of such results can be found in *e.g.*, chapter 6 of Duvaut and Lions (1976), or Frigaard (2019b).

3.3. Energy stability

This visco-plastic limit of the BMP model will also be globally energy stable under similar conditions to the analogous Bingham fluid flows. The energy equation is:

$$\frac{Re}{2}\frac{d}{dt}\langle \mathbf{u}^2\rangle = L(\mathbf{u}) - \langle \tau\dot{\gamma}(\mathbf{u})\rangle\,, \tag{29}$$

$$\leq -\frac{1}{2}\langle \dot{\gamma}^2(\mathbf{u})\rangle - [Y - Y_c]\langle \dot{\gamma}(\mathbf{u})\rangle\,, \tag{30}$$

with the same definition of Y_c. Physically the left hand side represents the growth in kinetic energy of a disturbance from zero, which is governed by the balance between energy input from forcing $L(\mathbf{u})$ and dissipation. We may then follow the analytical procedure in Karimfazli and Frigaard (2016), resulting in the following statement.

Provided $Y > Y_c$, as defined in Eq. (28), the BMP model with $\Lambda = W = 0$ is globally energy stable.

More explicitly, the kinetic energy $\langle \mathbf{u}^2\rangle$ decays monotonically to zero as $t \to \infty$ for any Re and any initial condition. There is a technical distinction between 2D and 3D, in that for 2D flows we can prove that the energy decay occurs in a finite time. The stopping time estimate can be estimated as in Karimfazli and Frigaard (2016), and will be very similar to that for the Bingham fluid, except noting that the viscous dissipation in the inequality following Eq. (29) is 0.5 times that for the Bingham fluid, *i.e.*, slightly slower decay for the BMP. For both fluids, if $Y >> 1$ the stopping time is inversely proportional to Y.

For $Y < Y_c$ we would expect there to be a steady flow. Energy stability methods can be used here, *e.g.*, resulting in something like a Reynolds-Orr equation for shear flows. These methods would also lead to an energy stability bound, but not independent of Re as we now have a transfer of kinetic energy from the base flow to the perturbation. Depending on the flow, this type of stability analysis might not be the most appropriate.

3.4. An alternate definition of Y_c

In many respects we have seen that the BMP model with $\Lambda = W = 0$ is analogous to the Bingham model in its behaviour. The slaving of the steady state fluidity to the strain rate (or dissipation, or stress) makes the above analysis relatively easy. It also allows for an alternate definition of Y_c. Using Eq. (19) we have:

$$\tau\dot{\gamma} = (Y^2 + \tau\dot{\gamma})\varphi_s = Y^2\varphi_s + \dot{\gamma}^2\,. \tag{31}$$

This suggest that an alternative definition of Y_c could come through the fluidity, *i.e.*,

$$Y_{c,a} = \sup_{\mathbf{v}\neq 0, \mathbf{v}\in V}\left\{\frac{L(\mathbf{v})}{\langle Y\varphi_s(\mathbf{v})\rangle}\right\}. \tag{32}$$

For the BMP model with $\Lambda = W = 0$, the relationship of φ_s to any velocity test function is well-defined and it seems that this definition of $Y_{c,a}$ would equivalently yield Y_c, but when we relax $\Lambda = 0$ or $W = 0$, this is less clear.

3.5. 1D Examples

We now present some 1D examples of the main points of the analysis, based on the plane Poiseuille flow of Fig. 1. With $\Lambda = W = 0$, we solve the transient problem:

$$Re\frac{\partial u}{\partial t} = f + \frac{\partial}{\partial y}\tau_{xy},\ y \in (-1,1),\ u(\pm 1,t) = 0\,. \tag{33}$$

We commence with a stopping flow, for which the initial conditions are $u(y, 0) = U(y)$, which is the solution of the plane Poiseuille flow in § 3.1 (the steady state of Eq. (33) with $f = 1$). For $t > 0$ we set $f = 0$, removing the driving pressure gradient and the velocity $u(y, t)$ decays to zero.

Numerically, we discretize using finite differences, second order in space and first order, fully implicit in time. Here we set mesh size $\Delta y = 0.01$ and use $\Delta t = \Delta y$ to compute. We use the augmented Lagrangian method to represent the unyielded regions correctly and iterate at each time step using an Uzawa algorithm. This is a standard method for solving Bingham fluid flows. For the BMP model we need to use $\varphi_s(|u_y|/Y)$ to eliminate τ_{xy}. This

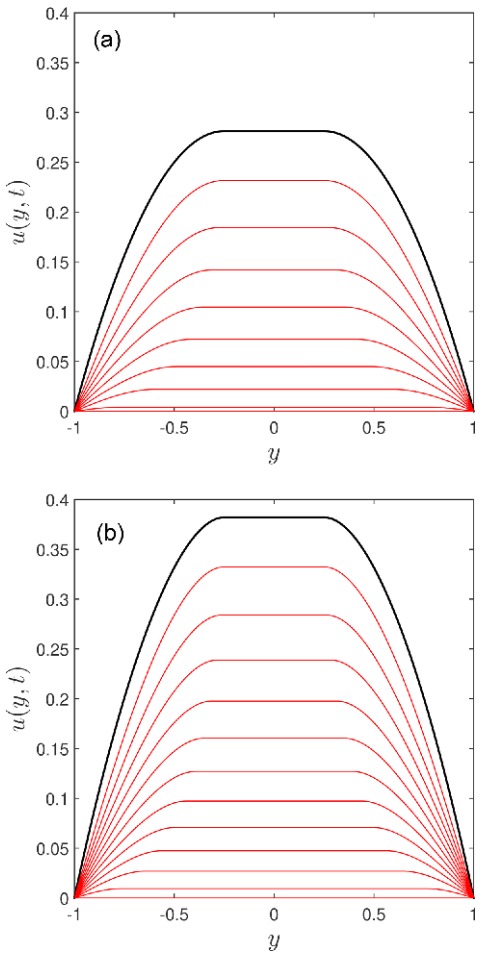

Fig. 3. (Color online) Stopping flow for: (a) Bingham fluid. (b) BMP with $\Lambda = W = 0$, both with $Y = 0.25$, and $Re = 1$. Initial condition (black) and profiles at intervals $Dt = 0.05$.

results in a nonlinear problem for the relaxed strain rate that is solved (numerically) at each step of the Uzawa loop (as opposed to the linear equation for the Bingham model), and hence a slower algorithm, but robust.

The results are shown in Fig. 3 comparing Bingham and BMP models at the same $Y = 0.25$. As expected, both converge monotonically to zero with the plug region widening progressively towards the walls. The Bingham fluid is more dissipative, has smaller initial velocity and converges to zero faster. Both decay in finite time, all as expected.

A second example shows startup flows, and only for the BMP model. Here an initial condition $u(y, 0)$ is set and for $t > 0$ we impose $f = 1$. Figure 4a illustrates the evolution from a random initial condition towards steady state, for $Y = 0.25$. Since here $Y < Y_c = 1$, there is a non-zero steady Poiseuille solution. The initial high frequencies are damped very quickly and we see convergence to the steady state. The time interval between velocity profiles is the same here as in the stopping flow of Fig. 3b. We see

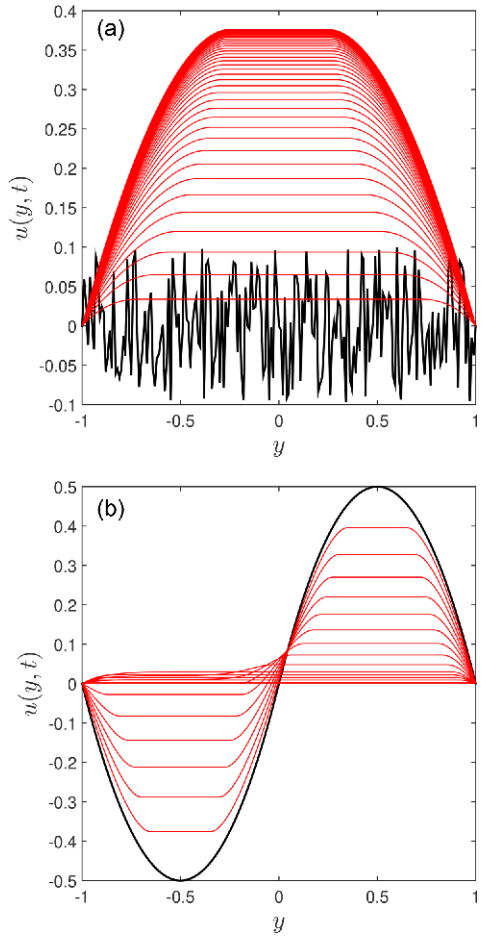

Fig. 4. (Color online) BMP flow with $\Lambda = W = 0$, $Re = 1$: (a) $Y = 0.25$ and startup flow from a random initial condition (black), profiles at intervals $Dt = 0.05$. (b) $Y = 1.5$ and startup flow from a cubic initial condition (black), profiles at intervals $Dt = 0.01$.

that convergence to the flowing steady state is slower than to the static state; the former decays exponentially. A different startup example is given in Fig. 4b which uses a cubic initial condition combined with $Y = 1.5$. The flow starts, but because $Y > Y_c$ it must converge to zero, which we observe.

4. Thixo-visco-plastic flows: $W = 0$

We now consider $\Lambda > 0$, but retain $W = 0$, *i.e.*, we consider thixo-visco-plastic (TVP) flows. We interpret these in the sense that the elastic timescale is much faster than the thixotropic and viscous timescales. As the flow is inelastic, Eq. (15) holds, from which we can eliminate either stress or strain rate tensors, and we may assume that $\underline{\underline{\boldsymbol{\tau}}} : \underline{\underline{\dot{\boldsymbol{\gamma}}}} \geq 0$. The kinetic equation, Eq. (11) measures time evolution of φ along a streamline. Therefore, approaching $\varphi = 0$ from above, the right-hand side of Eq. (15) is positive, and approaching $\varphi = 1$ from below, the right-hand side of Eq. (15) is negative. It follows that φ remains in [0,1].

The fluidity φ is no longer slaved to the local dissipation rate, but satisfies Eq. (11). Equation (11) requires boundary conditions for φ at any inflow. The velocity is non-zero only on $\partial\Omega_s$, on which the traction is specified. For example, in a duct flow we might specify the pressure drop. Although jumps in traction naturally occur in driving the flow, if we want to consider stability questions that involve φ, we would not expect any systematic input of fluidity. We thus restrict attention here to flows for which:

$$\int_{\partial\Omega_s} \varphi \mathbf{u} \cdot \mathbf{n} ds = 0 , \tag{34}$$

i.e., there is no net flux of fluidity into the flow region. Equation (34) is reasonable for example, in a steady Poiseuille flow where φ is constant in the stream wise direction. Alternatively, one might consider a periodically wavy channel in which φ also varies periodically between inflow and outflow.

4.1. Is Y still a yield stress?

Let us first consider to what extent this model remains viscoplastic, in the sense of a simple visco-plastic fluid. First suppose that the flow is steady:

$$\Lambda \mathbf{u} \cdot \nabla \varphi = \varphi \left[(1-\varphi) \frac{\tau^2}{Y^2} - 1 \right] . \tag{35}$$

The term $\Lambda \mathbf{u} \cdot \nabla \varphi$ is the evolution of φ along the streamline. We see that $\varphi = 0$ is one solution to Eq. (35). However, if $\varphi \neq 0$ then we see that φ evolves towards φ_s, as defined in the previous section by Eq. (17). If $\tau \leq Y$ then $\varphi \to \varphi_s = 0$ along the streamline. If $\tau > Y$ then $\varphi \to 1 - (Y/\tau)^2$ along the streamline, *i.e.*, again $\varphi = 0$ is not a stable solution for $\tau > Y$. Of course the flow is more complicated

now, as τ varies in the flow and hence also φ_s.

In this local analysis we see that Y is no longer a yield stress in the sense of a simple yield stress fluid. Instead Y is a threshold value that changes the limiting steady φ_s to fully structured for $\tau \le Y$. However, the fluidity φ continually chases φ_s along a streamline. If $\tau \le Y$, then $\varphi_s = 0$, but it not necessary that $\varphi = 0$ and hence $\dot{\gamma} \neq 0$ for $\tau \le Y$ is perfectly possible.

Let's now integrate Eq. (11) over Ω and use Eq. (15) to replace the dissipation rate with $\tau^2\varphi$:

$$0 = \int_{\partial\Omega_s} \varphi \mathbf{u}\cdot\mathbf{n} ds = \int_{\partial\Omega_s} \varphi \mathbf{u}\cdot\mathbf{n} ds + \int_{\partial\Omega_v} \varphi \mathbf{u}\cdot\mathbf{n} ds\,,$$

$$= \langle \nabla\cdot[\varphi\mathbf{u}]\rangle = \langle \mathbf{u}\cdot\nabla\varphi\rangle = \frac{1}{\Lambda}\langle\varphi\left[(1-\varphi)\frac{\tau^2}{Y^2}-1\right]\rangle\,. \tag{36}$$

Suppose now that $\tau \le Y$ everywhere in Ω. We see from Eq. (36) that the only way this may occur is if $\varphi = 0$ everywhere. In turn this implies that $\dot{\gamma} = 0$, using Eq. (15) and since the stress is finite. Thus, $\tau \le Y$ everywhere in Ω is sufficient to ensure the fluid is unyielded. Thus, to some extent Y acts as yield stress globally, in being a stress threshold below which the entire flow is unyielded.

However, in reverse order let us first suppose that $\dot{\gamma} = 0$. Using Eq. (15) we have $\varphi = 0$. We can infer that τ is at least bounded, but not directly that $\tau \le Y$. As argued previously, having $\tau > Y$ for $\varphi = 0$ is an unstable steady state for the kinetic equation.

If instead we suppose that the flow is not fully structured everywhere, Eq. (36) has an alternate interpretation. If we denote those regions where $\varphi = 0$ by Ω_0, we see that for the rest of the domain:

$$\int_{\Omega|\Omega_0} \varphi\left[(1-\varphi)\frac{\tau^2}{Y^2}-1\right] = 0\,. \tag{37}$$

Since $\varphi > 0$ in $\Omega|\Omega_0$, we see there is a (weighted) balance of regions with $\tau \le Y$ and with $\tau > Y$, in order for the above equation to hold. In other words, if $\varphi \neq 0$ we must have a combination of regions in which φ is evolving towards $\varphi_s = 0$ and those in which φ evolves towards $\varphi_s > 0$.

Including the time derivative of φ we see that $\langle\varphi\rangle$ is constantly evolving (over a timescale $\sim \Lambda$) towards a solution for which the right-hand-side of Eq. (36) is zero. Defining φ_s by using the local dissipation rate: $\varphi_s = \varphi_s(\tau\dot{\gamma}/Y^2)$, as in Eq. (19), and then subtracting off the steady state shows this explicitly:

$$\frac{d}{dt}\langle\varphi\rangle = \frac{1}{\Lambda}\langle(1+\tau\dot{\gamma}/Y^2)(\varphi_s-\varphi)\rangle\,. \tag{38}$$

Again φ chases φ_s in the above integral sense. This chasing of the steady state is common to many thixotropic models; see *e.g.*, the analysis and characterization in de Souza Mendes and Thompson (2012).

4.2. Static stability and Y_c

Although the yield stress interpretation is different for the TVP flow, formally at least we can still derive a type of critical yield value, relevant to stability.

Steady flows:

First let's consider a steady flow for which the total stress is bounded: $\tau < \tau_{\max}$. Using the mechanical energy balance we write:

$$0 \le \langle\dot{\gamma}^2(\mathbf{u})\rangle = L(\mathbf{u}) - \langle\tau\dot{\gamma}(\mathbf{u})\rangle + \langle\dot{\gamma}^2(\mathbf{u})\rangle\,. \tag{39}$$

From Eq. (36) and Eq. (15): $\langle\tau\dot{\gamma}\rangle = Y^2\langle\varphi\rangle + \langle\dot{\gamma}^2\rangle$, so that

$$0 \le \langle\dot{\gamma}^2(\mathbf{u})\rangle = L(\mathbf{u}) - Y^2\langle\varphi\rangle\,. \tag{40}$$

At this point it seems that we might use Eq. (32) and the alternate critical value $Y_{c,a}$ that we have discussed. However, φ is no longer slaved to $\dot{\gamma}$ and τ via the steady kinetic equation, so it is unclear if even $Y_{c,a} < \infty$.

Instead we use Eq. (15) to give $\dot{\gamma} = \tau\varphi$, and hence:

$$0 \le \langle\dot{\gamma}^2\rangle \le Y_c\langle\dot{\gamma}\rangle + -Y^2\langle\dot{\gamma}/\tau\rangle \le -\langle\dot{\gamma}\rangle\left(\frac{Y^2}{\tau_{\max}} - Y_c\right)\,. \tag{41}$$

with the definition of Y_c as before in Eq. (28). Therefore, for

$$Y \ge \sqrt{Y_c\,\tau_{\max}} \tag{42}$$

we guarantee that $\mathbf{u} = 0$ for the steady flow.

The format of the bound Eq. (42) is quite different to Eq. (28). Calculation of Y_c for simple yield stress fluids in general is dependent only on the distribution of the dimensionless forcing and/or boundary conditions, and on the shape of the flow domain Ω. It is not solution-dependent. We have also seen that in general the Y_c for the BMP model with $\Lambda = W = 0$ is identical with that of the Bingham fluid (or any other simple yield stress fluid).

The appearance of $\tau_{\max}$ in Eq. (42) means that the existence of the static steady state, $\mathbf{u} = 0$, depends on the stress distribution of the solution. However, in the case that the flow is static the stress distribution is indeterminate: Eq. (15) is satisfied but non-zero stress is possible where $\varphi = 0$. It is only necessary that the steady momentum balance is satisfied, which at most suggests that $\tau_{\max} = O(1)$ unless there are other flow constraints, *e.g.*, symmetry.

Transient flows:

To consider transients, we start first with the mean fluidity, which satisfies

$$Y^2\Lambda\frac{d}{dt}\langle\varphi\rangle + Y^2\langle\varphi\rangle = \langle(1-\varphi)\tau\dot{\gamma}\rangle = \langle\tau\dot{\gamma}\rangle - \langle\dot{\gamma}^2\rangle\,, \tag{43}$$

$$\le \tau_{\max}\langle\dot{\gamma}\rangle\,. \tag{44}$$

Using Eq. (43) in the energy equation:

$$\frac{Re}{2}\frac{d}{dt}\langle \mathbf{u}^2\rangle + \langle \tau\dot{\gamma}\rangle = L(\mathbf{u}), \tag{45}$$

$$\frac{Re}{2}\frac{d}{dt}\langle \mathbf{u}^2\rangle + Y^2\Lambda\frac{d}{dt}\langle \varphi\rangle = -\langle \dot{\gamma}^2\rangle + L(\mathbf{u}) - Y^2\langle \varphi\rangle,$$

$$\leq -\langle \dot{\gamma}^2\rangle - \langle \dot{\gamma}(\mathbf{u})\rangle\left(\frac{Y^2}{\tau_{\max}} - Y_c\right). \tag{46}$$

We focus mostly on the case $\tau_{\max} \geq Y_c$, since if $\tau_{\max} < Y_c$ then $Y > Y_c$ assures the steady state is static.

Before proceeding, note that $\tau_{\max}$ should now be considered as the supremum of τ over both Ω and temporally, from zero up to some end time t_{end}. As explained, the stress is not always determinate so we are making essentially a physical assumption that the stress is bounded. We brush past this point, noting that the aim here is to explain what we may expect in terms of stability rather than prove rigorous results.

Suppose now that $\tau_{\max} \geq Y_c$ and therefore $\sqrt{Y_c\tau_{\max}} \leq \tau_{\max}$. We consider the 3 different possibilities.

(i) If $Y \leq \sqrt{Y_c\tau_{\max}}$ there is no guarantee at all that we have a static steady state. Indeed if $Y < Y_c$ we see no mechanism for there to be a static steady state: we may of course have a flowing steady state. For $Y_c \leq Y < \tau_{\max}$, it is plausible that a steady state could be static or flowing. If the steady state were static, $\dot{\gamma}(\mathbf{u}) = 0$ and hence $\varphi = 0$, but since $Y < \tau_{\max}$ there will be some regions where $\varphi = 0$ and $\tau > Y$.

As discussed previously, such steady solutions are on the unstable branch of the kinetic equation, *i.e.*, φ grows when perturbed from zero. Although we neglected such transients previously (when $\Lambda = 0$), now we must allow a transient. These solutions correspond to flow with an avalanche effect, *i.e.*, a small perturbation will lead to increasing φ, which means non-zero $\dot{\gamma}$ and hence onset of motion. Since the right-hand side of Eq. (46) is not guaranteed to be negative, there is no decay of the kinetic energy, nor any other stability implied (under this analysis).

(ii) Suppose that $\sqrt{Y_c\tau_{\max}} < Y < \tau_{\max}$, in which case we have a static steady state: $\mathbf{u} = 0$, with $\dot{\gamma}(\mathbf{u}) = 0$ and hence $\varphi = 0$, for the steady state. Again since $Y < \tau_{\max}$ there will be some regions where $\varphi = 0$ and $\tau > Y$, and the kinetic equation is on the unstable branch. Thus, in parts of the flow domain we may see φ grow and an onset of motion. However, unlike (i), the energy equation is stable and Eq. (46) implies that the solution decays. Using Eq. (44) and the Poincaré inequality, we can write

$$\frac{d}{dt}\left[\frac{Re}{2}\langle \mathbf{u}^2\rangle + \Lambda Y^2\left(1 + \frac{Y^2}{\tau_{\max}^2} - \frac{Y_c}{\tau_{\max}}\right)\langle \varphi\rangle\right] \leq$$

$$-C_P\langle \mathbf{u}^2\rangle - Y^2\left(\frac{Y^2}{\tau_{\max}^2} - \frac{Y_c}{\tau_{\max}}\right)\langle \varphi\rangle, \tag{47}$$

where C_P is a constant in the Poincaré inequality. We see that the kinetic energy plus a linear multiple of $\langle \varphi\rangle$ will decay exponentially to zero. If we write:

$$\alpha_1 = \frac{2Y^2\Lambda}{Re}\left(1 + \frac{Y^2}{\tau_{\max}^2} - \frac{Y_c}{\tau_{\max}}\right),\ \alpha_2 = \frac{1}{C_P}\left(\frac{Y^2}{\tau_{\max}^2} - \frac{Y_c}{\tau_{\max}}\right), \tag{48}$$

it becomes straightforward to derive the following conditions.

If $\alpha_1 \leq \alpha_2$, then $\lambda_1 = 2C_P/Re$ and

$$[\langle \mathbf{u}^2\rangle + \alpha_1\langle \varphi\rangle](t) \leq [\langle \mathbf{u}^2\rangle + \alpha_1\langle \varphi\rangle](0)e^{-\lambda_1 t}. \tag{49}$$

If $\alpha_1 \leq \alpha_2$, then $\lambda_2 = 2C_P\alpha_2/(Re\,\alpha_1)$ and

$$\left[\frac{1}{\alpha_1}\langle \mathbf{u}^2\rangle + \langle \varphi\rangle\right](t) \leq \left[\frac{1}{\alpha_1}\langle \mathbf{u}^2\rangle + \langle \varphi\rangle\right](0)e^{-\lambda_2 t}. \tag{50}$$

Note that for the first case the decay timescale has $t \sim O(Re)$ and for the second $t \sim O(\Lambda)$, with $\alpha_1 \geq \alpha_2$ for larger Λ, *i.e.*, the slowest timescale governs. Similar energy bounds can be obtained by other means (with slightly different constants), but have in common this switch in timescales.

This decay is monotone but allows for transient growth locally as has been described. Qualitatively, this corresponds to an energetically repressed avalanche effect in which any flow onset is short-lived and the flow returns to a fully structured static state. Since the dissipation rate remains positive throughout, the motion dissipates energy. Physically, we might expect the new state to have smaller stress, but we cannot prove this.

(iii) Finally, suppose that $Y > \tau_{\max}$. Then we again have a static solution with $\varphi = 0$. However, if now there is any perturbation then φ decays monotonically to 0, both locally Eq. (11), and in the mean - rearranging Eq. (43). Thus, the avalanche effect behaviour is not found: the fluid becomes structured everywhere for large enough Y. The same energy inequalities as above can be used.

Remarks:

An interesting point for (ii) and (iii) is that although the flow is energy stable, we lose the finite time decay as soon as $\Lambda > 0$. To see this, suppose that $\mathbf{u} = 0$ after a finite time. Since then $\dot{\gamma}(\mathbf{u}) = 0$, we see that also $\varphi = 0$. However, this contradicts Eq. (43), which has at most exponential decay, *i.e.*, the right-hand side is always positive. Thus, even if the kinetic energy wants to decay faster, the structure build-up inherent in the fluidity equation will retard it. Although the decay bounds are exponential, these are conservative bounds. Viewed naively, the term $-\langle \dot{\gamma}^2/\varphi\rangle$ leads to a stabilizing viscous diffusion, with diffusivity $1/\varphi$. Thus, we expect the stability to accelerate as $\varphi \to 0$.

We have also lost the global stability, although this may not be explicitly obvious. Since our stability criteria on Y now involve $\tau_{\max}$ there will be dependence on the initial state of stress, even assuming that the stresses decay with

the velocity. It is interesting to reflect that all the distinctions above in (i) - (iii) arise from the state of stress, *i.e.*, $\tau_{\max}$. In a simple yield stress fluid τ would be indeterminate below the yield stress. Here, we have not actually removed the indeterminacy (for $W = 0$). It is frustrating that we only can discuss and describe stability via $\tau_{\max}$, but have no means of estimating $\tau_{\max}$ in a static fluid.

Pragmatically then, what can we say? If the flow domain gives you no reason to expect any stress singularity, it could be reasonable to assume a bound such as $\tau_{\max}$. Although the bound might be unknown, knowledge of the driving forces of the flow may help to estimate reasonably. Then taking Y large enough, *i.e.*, satisfying Eq. (42), should result in a exponential decay to zero of both the kinetic energy and the mean fluidity. The fluidity decay is no faster than exponential but kinetic energy decay is probably faster. Depending on whether viscous or kinetic timescale is faster, we have different exponential decay rates.

For the TVP problem with $\Lambda > 0$, the value $\tau = Y$ does not represent a yield stress in the same local way as in a simple yield stress fluid. Instead Y is a threshold stress value that changes the limiting steady φ_s from zero to positive as τ increases through Y. The simple yield stress fluid interpretation is recovered only as $\Lambda \to 0$ when $\varphi \to \varphi_s$ rapidly.

4.3. 1D Examples

We again present some 1D examples of the main points of the analysis, based on the plane Poiseuille flow. Throughout we fix $Re = 1$, so that we can compare solutions in which the kinetics of the fluidity evolve fast ($\Lambda < 1$) or slow ($\Lambda > 1$), *i.e.*, relative to the viscous timescale.

We may eliminate the stress in both momentum and kinetic equations. However, the divide through by φ is problematic as $\varphi \to 0$. It might be possible to use an augmented Lagrangian technique again to circumvent this, but here we simply regularize the viscosity terms. The system of equations to be solved is

$$Re\frac{\partial u}{\partial t} = f + \frac{\partial}{\partial y}\left[\frac{1}{\varphi_R}\frac{\partial u}{\partial y}\right],\ y \in (-1,\ 1),\ u(\pm 1,\ t) = 0\,, \tag{51}$$

$$\Lambda\frac{\partial \varphi}{\partial t} = -\varphi + \frac{(1-\varphi)}{Y^2\varphi_R}\left[\frac{\partial u}{\partial y}\right]^2, \tag{52}$$

where $\varphi_R = (\varphi^2 + \varepsilon^2)^{1/2}$ and $\varepsilon << 1$. This regularization affects only the plug regions. The equations are now solved numerically, discretized using finite differences, fully implicit in time and second order in y.

The first example repeats the stopping problem of the VP flow, for $Y = 0.25$. The initial condition is the BMP Poiseuille flow velocity profile ($f = 1$) and associated steady state fluidity φ_s. For $t > 0$ we set $f = 0$ so that the flow decays. For $\Lambda = 10$ (see Fig. 5), the fluidity kinetics

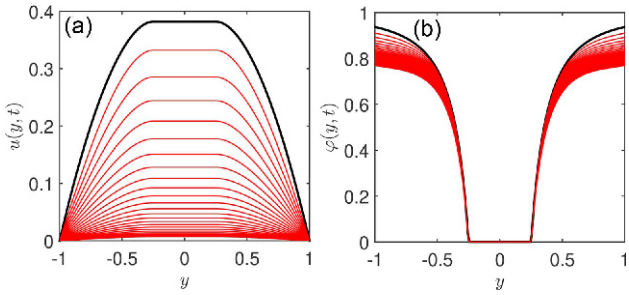

Fig. 5. (Color online) Stopping flow for an inelastic BMP fluid with $Y = 0.25$, $Re = 1$, $W = 0$, and $\Lambda = 10$: (a) velocity and (b) fluidity. Initial profiles in black, profiles at intervals $Dt = 0.05$.

are slow and the velocity decays to zero faster. We observe that the velocity is practically zero when the fluidity has hardly changed from its initial profile. The computation is repeated for various ε and we found little change for $\varepsilon < 10^{-3}$ and this value essentially only influences the low fluidity threshold within the plug region. We have used $\varepsilon < 10^{-4}$ for all computations thereafter.

In contrast, Fig. 6 shows the same flow except $\Lambda = 0.1$. We show solution profiles initially with time spacing $Dt = 0.005$ (red) and then later $Dt = 0.05$ (blue). We observe a very rapid decay in φ away from the initial condition. The fluidity then appears to track the steady state fluidity φ_s, as defined by the slowly evolving velocity gradient. Decay of the velocity is the controlling rate. Note however that the velocity decay is still faster than that of Fig. 5, since the decaying fluidity contributes to accelerate the kinetic energy decay. It almost seems that the decay is in finite time, although on close inspection we have a viscous decay controlled by the regularized minimum fluidity ε.

For $\Lambda < 1$, we observe that φ remains largest at $y = \pm 1$ and decays monotonically. As the dissipation becomes very small we might expect that the first term in the kinetic equation dominates, so that $\varphi(\pm 1,\ t) \sim \varphi(\pm 1,\ 0)\ \exp(-t/\Lambda)$. In this case we might expect that $u(y,\ t)$ decays

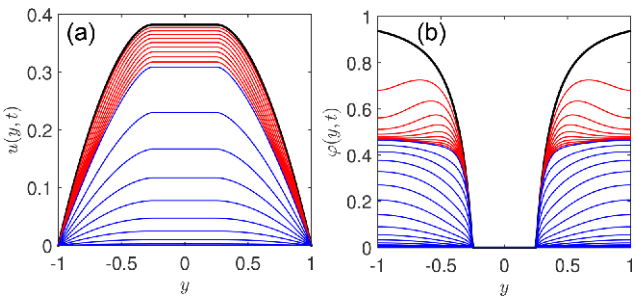

Fig. 6. (Color online) Stopping flow for an inelastic BMP fluid with $Y = 0.25$, $Re = 1$, $W = 0$, and $\Lambda = 0.1$: (a) velocity and (b) fluidity. Initial profiles in black, profiles at intervals $Dt = 0.005$ (red) and $Dt = 0.05$ (blue).

faster than the solution $v(y, t)$ of:

$$Re\frac{\partial v}{\partial t} = \frac{e^{t/\Lambda}}{\varphi(\pm 1, 0)}\frac{\partial^2 v}{\partial y^2}, y \in (-1, 1), v(\pm 1, t) = 0\,. \tag{53}$$

For this problem, as it is separable, we can find series solutions. The slowest modes decay like:

$$v(y, t) \sim e^{-[\pi^2\Lambda/Re\,\varphi(\pm 1, 0)]e^{t/\Lambda}}, \tag{54}$$

as $t \to \infty$. Thus, we see that (doubly) exponential decay might be expected for stopping flows with small Λ.

Next we consider starting flows. As an initial state we take a fully developed Newtonian Poiseuille flow velocity, (for $f = 1$), and as fluidity, $\varphi(y, t) = 1$. For $Y = 0.25$ there is a non-zero steady Poiseuille solution with a central plug, as we have seen earlier in the paper. The solutions converge to this steady state velocity and associated steady fluidity $\varphi_s(y)$. The convergence is again controlled by the slower timescale. For $\Lambda = 10$ (Fig. 7), the velocity converges quickly and the fluidity retards this. For $\Lambda = 0.1$ (Fig. 8), the fluidity converges quickly and the velocity retards convergence. Because neither final state is zero, the convergence appears to remain on the exponential timescales suggested by our analysis.

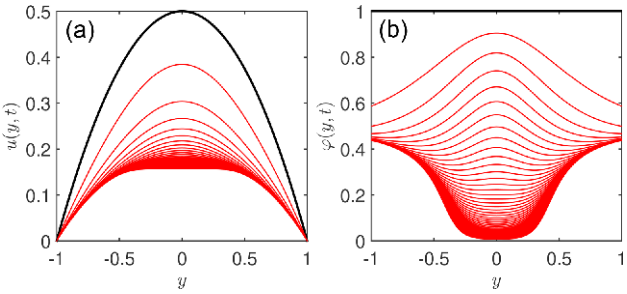

Fig. 7. (Color online) Convergence to Poiseuille flow for an inelastic BMP fluid with $Y = 0.25$, $Re = 1$, $W = 0$, and $\Lambda = 10$: (a) velocity and (b) fluidity. Initial profiles in black, (Newtonian parabolic velocity profile and fluidity $\varphi = 1$). Profiles at intervals $Dt = 1$.

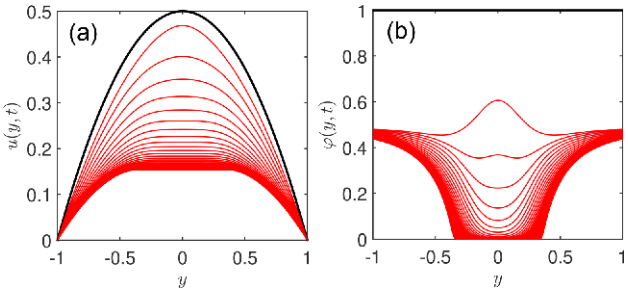

Fig. 8. (Color online) Convergence to Poiseuille flow for an inelastic BMP fluid with $Y = 0.25$, $Re = 1$, $W = 0$, and $\Lambda = 0.1$: (a) velocity and (b) fluidity. Initial profiles in black, (Newtonian parabolic velocity profile and fluidity $\varphi = 1$). Profiles at intervals $Dt = 0.05$.

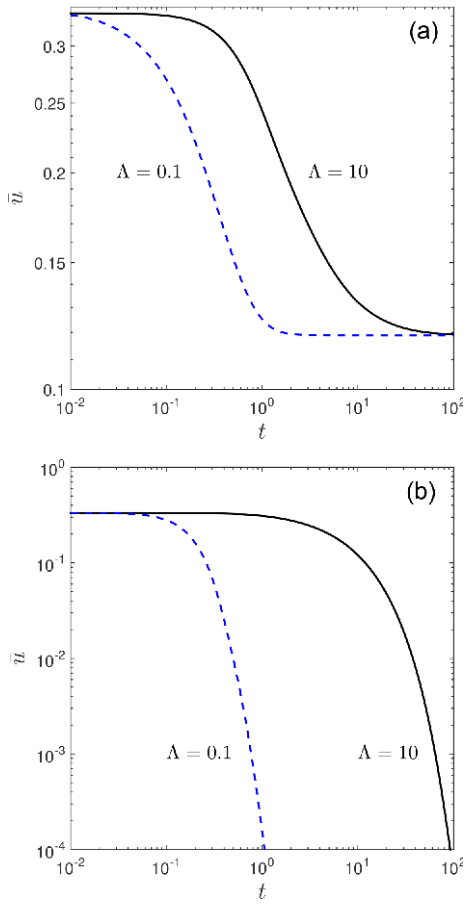

Fig. 9. (Color online) Convergence of mean velocity for: (a) $Y = 0.25$, results of Figs. 7 and 8. (b) $Y = 1.5$, other parameters as in Figs. 7 and 8.

Figure 9a shows the convergence of the mean velocity to the steady state in the two cases, converging for $t \sim 10$ for $\Lambda = 10$ (structure controls: $t \sim \Lambda$), and converging for $t \sim 1$ for $\Lambda = 0.1$ (viscosity controls: $t \sim Re = 1$). On setting $Y = 1.5 > Y_c$ there is only the static steady solution. Both cases decay rapidly to zero, again controlled by the slowest timescale; see Fig. 9b. Particularly for $\Lambda = 0.1$ the decay appears very rapid compared to the (high shear) viscous timescale, $t \sim Re$. Since for small φ we have regularised to limit the viscosity to ε^{-1} the final decay of the velocity is exponential.

Lastly we explore whether we can have a super-stressed initial profile when static and fully structured. Here we impose an initial stress: $\tau_{xy} = -1-y$, which gives $\tau_{\max} = 2$, we have $Y_c = 1$ and set $Y = 1.5$. Therefore, we find $y > \sqrt{2} = \sqrt{Y_c\,\tau_{\max}}$. We also set $\varphi = u = 0$ initially. Theoretically, these initial conditions should admit a steady state, albeit unstable to small perturbations for $|\tau_{xy}| > Y$. The difficulty numerically is that although setting $\varphi = u = 0$ is fine, the stress would not then be defined. To circumvent this, we have regularized the fluidity expression where it might be singular, but this itself leads to a rapid change from the

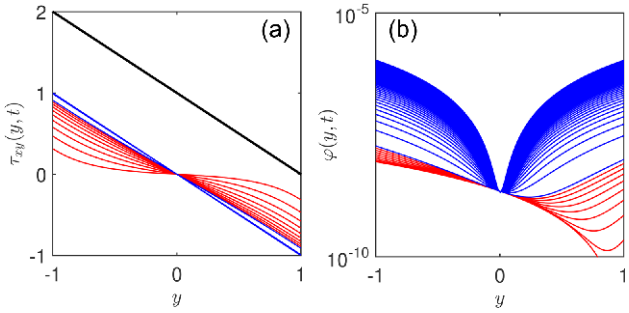

Fig. 10. (Color online) Effects of an super-stressed initial profile when static and fully structured: inelastic BMP fluid with $Y = 1.5$, $Re = 1$, $W = 0$, and $\Lambda = 0.1$ Early time evolution: (a) stress and (b) fluidity. Initial profiles in black, ($\tau_{xy} = -1-y$, $\varphi = u = 0$; profiles at intervals $Dt = 10^{-5}$ (red) and $Dt = 10^{-4}$ (blue).

initial state. In other words, the regularization provides an initial perturbation from the steady state. Figure 10 shows evolution of the stress and fluidity from these initial conditions. There is a rapid change in the stress near $y = -1$, dropping below the symmetric steady state value and then rebounding and converging. The fluidity (and velocity) also have a brief transient but then converge to zero (meaning to very small equilibrium values determined by the regularization).

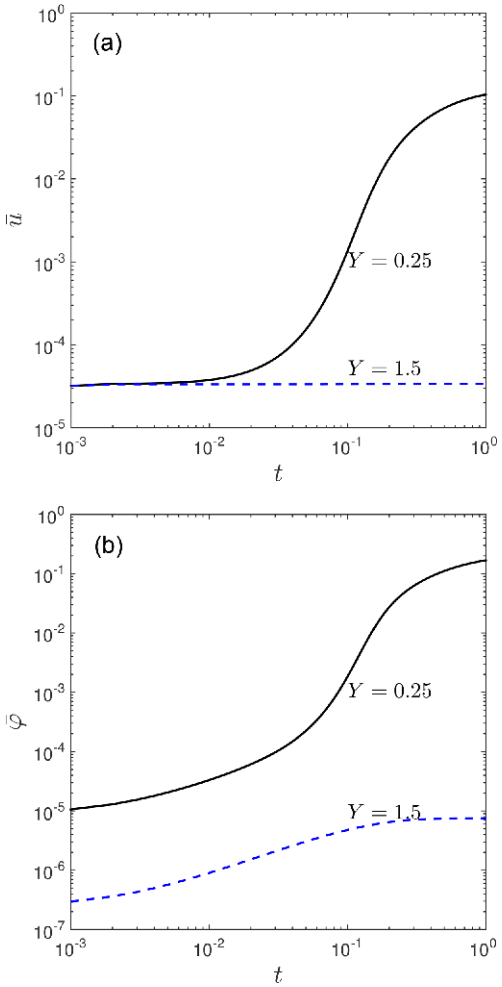

Fig. 11. (Color online) Variations in: (a) mean velocity; (b) mean fluidity, for flow of Fig. 10 with $Y = 0.25$ (restart) and $Y = 1.5$ (no restart).

For smaller Y, *i.e.*, $Y < 1$ here, the restart process continues and the flows converge to a steady flow. There is some initial asymmetry in the flow due to the initial stress but short lived. The convergence of the mean velocity and mean fluidity are illustrated in Fig. 11. Unfortunately, within the scope of a simple 1D example with the regularization used, it does not easy to explore the different possibilities we have discussed.

5. Elasto-visco-plastic flows: $\Lambda = 0$

In the elasto-visco-plastic (EVP) limit we assume thixotropic evolution is faster than elastic, with the interpretation that $W >> \Lambda \sim 0$. Thus, Eqs. (8) and (10) are satisfied and Eq. (11) is replaced by:

$$\varphi = (1 - \varphi)\frac{\underline{\underline{\boldsymbol{\tau}}}:\underline{\underline{\dot{\boldsymbol{\gamma}}}}}{Y^2}. \tag{55}$$

Although by definition the fluidity should remain bounded between 0 and 1, in a viscoelastic fluid there is no guarantee that the dissipation above is positive. Indeed, in classical oscillatory shear, the elastic and viscous responses are out of phase. If the dissipation term is negative then $\varphi < 0$, which is unphysical. To remedy this, we might either consider only a part of the total stress, such that the dissipation is semi-positive, or alternately we may take the absolute value above:

$$\varphi = (1 - \varphi)\frac{|\underline{\underline{\boldsymbol{\tau}}}:\underline{\underline{\dot{\boldsymbol{\gamma}}}}|}{Y^2}, \tag{56}$$

which on rearranging gives us:

$$|\underline{\underline{\boldsymbol{\tau}}}:\underline{\underline{\dot{\boldsymbol{\gamma}}}}| = \frac{Y^2\varphi}{1-\varphi}, \; \varphi = \frac{|\underline{\underline{\boldsymbol{\tau}}}:\underline{\underline{\dot{\boldsymbol{\gamma}}}}|}{Y^2 + |\underline{\underline{\boldsymbol{\tau}}}:\underline{\underline{\dot{\boldsymbol{\gamma}}}}|}. \tag{57}$$

Note that the upper convected derivative term in Eq. (10), for $W \neq 0$, prevents us from switching to using the stress or strain rate as alternatives in defining φ.

5.1. Local yielding behaviour

Local yielding behaviour in the BMP model comes from the kinetic equation, which is in steady state here. On rewriting Eq. (56) as:

$$\varphi\left[(1-\varphi)\frac{|\underline{\underline{\boldsymbol{\tau}}}:\underline{\underline{\dot{\boldsymbol{\gamma}}}}|}{\varphi Y^2} - 1\right] = 0, \tag{58}$$

we see that if $|\underline{\underline{\boldsymbol{\tau}}}:\underline{\underline{\dot{\boldsymbol{\gamma}}}}|/\varphi \leq Y^2$ then the only solution is $\varphi = 0$. For $W \neq 0$ we cannot use Eq. (10) to switch this into a condition on the stress. Lets then look at the implications.

First, returning to Eq. (56) we see that $\varphi = 0$ implies that $|\underline{\underline{\tau}}:\underline{\underline{\dot{\gamma}}}| = 0$. Assuming that $|\underline{\underline{\tau}}:\underline{\underline{\dot{\gamma}}}|/\varphi \le Y^2$ means we consider a limit in which $|\underline{\underline{\tau}}:\underline{\underline{\dot{\gamma}}}| = O(\varphi)$ as $\varphi \to 0$. We also see from Eq. (57) that $\varphi = 0(|\underline{\underline{\tau}}:\underline{\underline{\dot{\gamma}}}|)$ as $|\underline{\underline{\tau}}:\underline{\underline{\dot{\gamma}}}| \to 0$.

It follows that the yield condition $|\underline{\underline{\tau}}:\underline{\underline{\dot{\gamma}}}|/\varphi \le Y^2$ can be satisfied with finite τ and allowing $\dot{\gamma} \sim \varphi = 0$. This distinguished limit gives rise to a type of yield stress behaviour, except that the limiting stress is not determined in this limit. Indeed, other possibilities are not refuted. For example $|\underline{\underline{\tau}}:\underline{\underline{\dot{\gamma}}}| = 0$ can be satisfied with non-zero stress and strain rate.

5.2. Static steady states

Let us now consider steady flows for which we will decompose: $\underline{\underline{\tau}} = \underline{\underline{\tau}}^v + \underline{\underline{\tau}}^e$, where for $\underline{\underline{\tau}}^v$ we simply take the viscous part of the stress, *i.e.*,

$$\underline{\underline{\tau}}^v = \underline{\underline{\dot{\gamma}}}/\varphi \,. \tag{59}$$

To start with we will assume that $\underline{\underline{\tau}}^e : \underline{\underline{\dot{\gamma}}} = 0$.

Note we can always write $\underline{\underline{\tau}}^v$ in this way, but there is no guarantee that $\underline{\underline{\tau}}^e : \underline{\underline{\dot{\gamma}}} = 0$. This assumption does hold for an important class of flows: uniform duct flows. For example, in a fully developed flow along a duct with uniform cross-section in the (y, z)-plane, we have a single velocity component $u(y, z)$ and:

$$\tau^v_{xy} = \tau^v_{yx} = \frac{1}{\varphi}\frac{\partial u}{\partial y},\ \tau^v_{xz} = \tau^v_{zx} = \frac{1}{\varphi}\frac{\partial u}{\partial z}, \tag{60}$$

with $\tau^v_{ij} = 0$ otherwise. We can then construct the steady components of $\underline{\underline{\tau}}^e$:

$$\tau^e_{xx} = \frac{2W}{\varphi}\left[\left(\frac{\partial u}{\partial y}\right)^2 + \left(\frac{\partial u}{\partial z}\right)^2\right], \tag{61}$$

and $\tau^e_{ij} = 0$ otherwise.

With the above assumption that $\underline{\underline{\tau}}^e : \underline{\underline{\dot{\gamma}}} = 0$, we find that

$$\varphi = (1-\varphi)\frac{\tau^v\dot{\gamma}}{Y^2} = \varphi(1-\varphi)\frac{(\tau^v)^2}{Y^2} = (1-\varphi)\frac{\dot{\gamma}^2}{\varphi Y^2} \tag{62}$$

and the condition $|\underline{\underline{\tau}}:\underline{\underline{\dot{\gamma}}}|/\varphi \le Y^2$ is simply $\tau^v \le Y$, *i.e.*, a yield criterion based on the viscous part of the stress. Furthermore, the above identities are analogous to those in § 3 for the steady φ_s: slaved to the stress, dissipation or strain rate (except here using τ^v).

It follows that when $\underline{\underline{\tau}}^e : \underline{\underline{\dot{\gamma}}} = 0$, we may construct the steady mechanical energy balance as before, substitute for the dissipation and conclude that for $Y \ge Y_c$, as defined by Eq. (28), we have $\mathbf{u} = 0$. In other words we have the same critical yield limit for the steady EVP flow, provided that $\underline{\underline{\tau}}^e : \underline{\underline{\dot{\gamma}}} = 0$, *e.g.*, for uniform duct flows. Additionally, in the previous subsection we can readily see that Y plays the local role of a yield stress, *i.e.*, $\tau^v \le Y$ implies that $\dot{\gamma} = 0$.

5.3. Flows with $\underline{\underline{\tau}}^e : \underline{\underline{\dot{\gamma}}} \neq 0$

Now let's examine if we can remove the constraint $\underline{\underline{\tau}}^e : \underline{\underline{\dot{\gamma}}} = 0$. From Eq. (10) for a steady flow, we find $\underline{\underline{\tau}}^e$, which is given componentwise by:

$$\tau^e_{ij} = \frac{W}{\varphi}\left[-u_j\frac{\partial}{\partial x_j}\tau_{ij} + \frac{\partial u_i}{\partial x_k}\tau_{kj} + \frac{\partial u_j}{\partial x_k}\tau_{ik}\right]. \tag{63}$$

Thus, we see that $\underline{\underline{\tau}}^e \sim O(W)$ and for bounded stress fields:

$$\underline{\underline{\tau}}^e : \underline{\underline{\dot{\gamma}}} \sim O(W|\mathbf{u}|\dot{\gamma}/\varphi) + O(W\dot{\gamma}^2/\varphi)\,. \tag{64}$$

For small W we may expand $|(\underline{\underline{\tau}}^v + \underline{\underline{\tau}}^e):\underline{\underline{\dot{\gamma}}}|$ in terms of W, *i.e.*,

$$|(\underline{\underline{\tau}}^v + \underline{\underline{\tau}}^e):\underline{\underline{\dot{\gamma}}}| = \tau^v\dot{\gamma}\left[1 + \frac{\underline{\underline{\tau}}^e:\underline{\underline{\dot{\gamma}}}}{\tau^v\dot{\gamma}}\right] \sim \tau^v\dot{\gamma}[1 + O(W)]\,. \tag{65}$$

We now formulate the steady mechanical energy balance, retaining $\underline{\underline{\tau}}^e$

$$0 = L(\mathbf{u}) - \langle(\tau^v)^2\varphi\rangle - \langle\underline{\underline{\tau}}^e : \underline{\underline{\dot{\gamma}}}\rangle\,. \tag{66}$$

We now denote by $\varphi_s(\tau^v)$ the function defined by (62). We can write $\varphi = \dfrac{\tau^v\dot{\gamma}[1 + (\underline{\underline{\tau}}^e:\underline{\underline{\dot{\gamma}}}/\tau^v\dot{\gamma})]}{[Y^2 + \tau^v\dot{\gamma}][1 + (\underline{\underline{\tau}}^e:\underline{\underline{\dot{\gamma}}}/\tau^v\dot{\gamma})]/[Y^2 + \tau^v\dot{\gamma}]}$, and then expand in a series, assuming $(\underline{\underline{\tau}}^e:\underline{\underline{\dot{\gamma}}}/\tau^v\dot{\gamma}) << 1$:

$$\varphi = \varphi_s + \varphi_s^2\left(\frac{\underline{\underline{\tau}}^e:\underline{\underline{\dot{\gamma}}}}{\tau^v\dot{\gamma}}\right) - \frac{\varphi_s^2 Y^2}{Y^2 + \tau^v\dot{\gamma}}\left(\frac{\underline{\underline{\tau}}^e:\underline{\underline{\dot{\gamma}}}}{\tau^v\dot{\gamma}}\right)^2 + \ldots \tag{67}$$

Combining with Eq. (66) and ignoring second order terms we have:

$$\begin{aligned} 0 &= L(\mathbf{u}) - \langle(\tau^v)^2\varphi_s\rangle - \langle(\varphi_s + 1)\underline{\underline{\tau}}^e : \underline{\underline{\dot{\gamma}}}\rangle \\ &\le Y_c\langle\dot{\gamma}\rangle - \langle\dot{\gamma}^2/\varphi_s(\dot{\gamma}/Y)\rangle - \langle(\varphi_s + 1)\underline{\underline{\tau}}^e : \underline{\underline{\dot{\gamma}}}\rangle\,, \end{aligned} \tag{68}$$

as in Eq. (25).

The first two terms are exactly as in our analysis of the viscoplastic limit ($\Lambda = W = 0$). These may be combined and bounded above by: $-(Y - Y_c)\langle\dot{\gamma}\rangle - \frac{1}{2}\langle\dot{\gamma}^2\rangle$.

These terms are linear in the velocity and strain rate as $\dot{\gamma} \to 0$. The third term, for bounded stress is also linear in W times the velocity or the strain rate.

In order to preserve a static steady state, it seems that we need to balance these convective stress contributions with increased plastic dissipation. In other words, if $\underline{\underline{\tau}}^e : \underline{\underline{\dot{\gamma}}} \neq 0$, a steady state will be static ($\mathbf{u} = 0$), provided that:

$$Y > Y_c + C_s W\,, \tag{69}$$

where $C_s > 0$ will depend linearly on assumed bounds for the total stress and stress gradients. In other words there can be an additional elastic component to the critical Y_c that needs to be exceeded. This component scales linearly with W for small W. There are likely classes of flows *e.g.*, slowly varying wavy channels, for which the elastic con-

tribution C_s could be estimated. On the other hand, there are possibly elastic flows with singularities that would not be admissible and violate Eq. (69).

5.4. Comments

The bound Eq. (69) is really only intended to highlight some of the difficulties in establishing even a steady flow result. Compared to the VP limit we have lost the sharpness of the bound Y_c and still need bounds on the stress and gradients. We have not succeeded to derive any stability results for the transient problem. If such a result were established, it appears that it would also not be global.

5.5. 1D Examples

We again present some examples based on the plane Poiseuille flow. The flow is 1D and the system solved is:

$$Re\frac{\partial u}{\partial t} = f + \frac{\partial}{\partial y}\tau_{xy},\ y \in (-1,\ 1),\ u(\pm 1,\ t) = 0\,, \tag{70}$$

$$W\frac{\partial \tau_{xy}}{\partial t} = \frac{\partial u}{\partial y} - \varphi\tau_{xy}\,, \tag{71}$$

$$\varphi = \frac{\left|\tau_{xy}\dfrac{\partial u}{\partial y}\right|}{Y^2 + \left|\tau_{xy}\dfrac{\partial u}{\partial y}\right|}\,. \tag{72}$$

We use a staggered mesh, with τ_{xy} and φ approximated at half-meshpoints and u at full meshpoints. The time advance is done with a predictor-corrector scheme. The timestep is selected to satisfy a CFL constraint for the underlying hyperbolic problem, *i.e.*, $\Delta t < \Delta y\sqrt{ReW}$.

We commence with two stopping flows for $\Lambda = 0$ and $Re = 1$. Initial conditions are the plane Poiseuille flow solution with $Y = 0.25$. We solve for both $W = 0.1$ and $W = 10$, to contrast the near inelastic with the strongly elastic. Since for $t > 0$ we set $f = 0$, there is no driving force for the flow. Evidently $u = 0$ is now a steady solution, but the question is how the solution variables converge.

In Fig. 12 we see the solution for $W = 0.1$. The velocity drops from its initial condition, but not monotonically. Near the wall the initially concave velocity profile becomes convex and the velocity overshoots, becoming negative before again accelerating. Similarly, the stress gradient changes from negative to positive, away from the walls, and oscillates.

The oscillations are significantly larger for $W = 10$; see Fig. 13. Here the velocity oscillations dwarf the initial velocity. They are driven by the oscillating stress. In both cases these are damped elastic waves, as can be seen by eliminating the stress equation:

$$ReW\frac{\partial^2 u}{\partial t^2} = \frac{\partial^2 u}{\partial y^2} - \frac{\partial}{\partial y}[\varphi\tau_{xy}]\,. \tag{73}$$

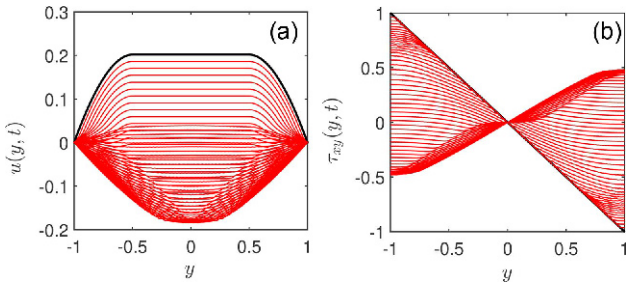

Fig. 12. (Color online) Stopping flow for non-thixotropic BMP fluid with $Y = 0.25$, $Re = 1$, $\Lambda = 0$, and $W = 0.1$: (a) velocity; (b) stress. Initial profiles in black; profiles at intervals $Dt = 0.0158$.

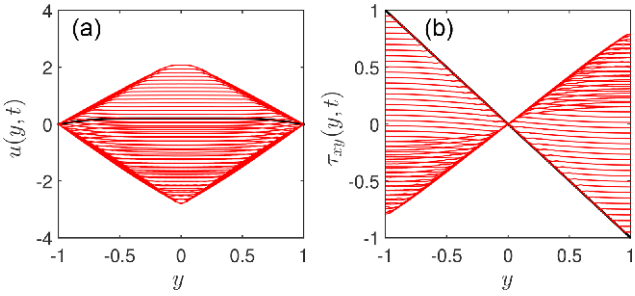

Fig. 13. (Color online) Stopping flow for non-thixotropic BMP fluid with $Y = 0.25$, $Re = 1$, $\Lambda = 0$, and $W = 10$: (a) velocity; (b) stress. Initial profiles in black; profiles at intervals $Dt = 0.158$.

On using Eq. (70) we can see that the final term contains a damping term: $\varphi\dfrac{\partial \tau_{xy}}{\partial y} = Re\,\varphi\dfrac{\partial u}{\partial t}$.

Figure 14 shows the decay of the mean velocity with time for the results of Figs. 12 and 13. The wave speed of the undamped system is $1/\sqrt{ReW}$, which corresponds to the timescale we observe for the oscillations, travelling over distance 1. Strangely the damping term is less active as $\varphi \to 0$, which has the effect of prolonging the oscillations. An interpretation of this is that for zero fluidity, the yield stress limit is wholly elastic, *i.e.*, the damping would vanish. This suggests that a stopping flow may be a useful viscometric flow with which to test materials that one expects to represent with the BMP model.

We now explore the starting flows, in which the fluids are initially stationary and then $f = 1$ is applied for $t > 0$. Again we fix $\Lambda = 0$, $Re = 1$, and $Y = 0.25$ and solve for $W = 0.1$ and $W = 10$. The relatively inelastic flow is observed to converge rapidly and monotonically to the Poiseuille profile; see Fig. 15. Initially the core of the fluid is accelerated uniformly by the pressure gradient, with viscous effects diffusing in from the walls (red profiles). This then fills out as the Poiseuille profile is approached.

In contrast, for $W = 10$ we again see large scale elastic oscillations in positive and negative directions, as illustrated in Fig. 16. These oscillations are damped and eventually this flow also converges to the plane Poiseuille

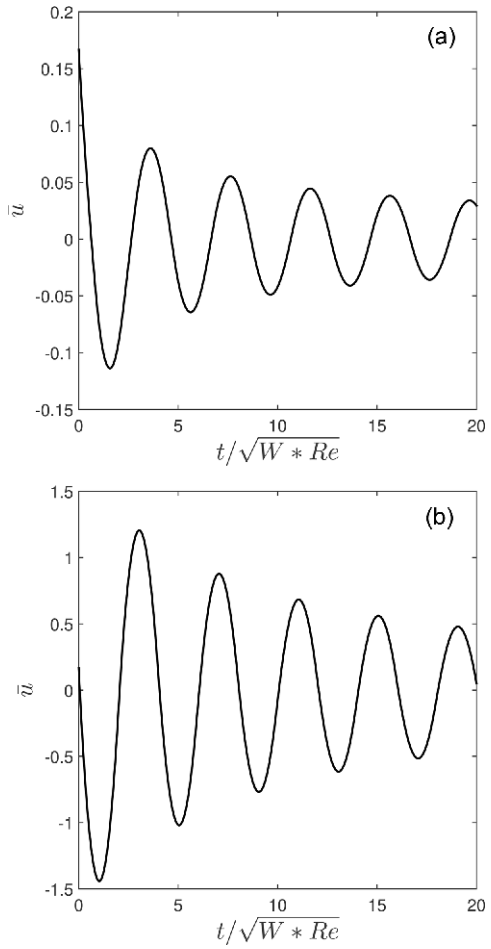

Fig. 14. Variations in mean velocity with time for: (a) Fig. 12; (b) Fig. 13.

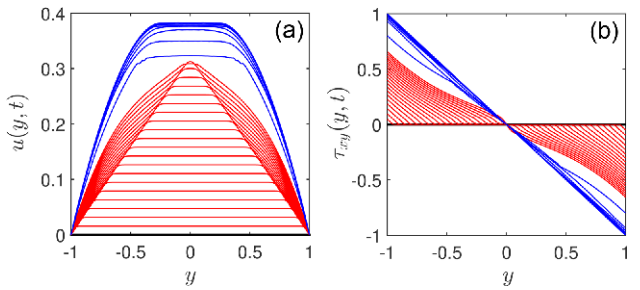

Fig. 15. (Color online) Startup flow for non-thixotropic BMP fluid with $Y = 0.25$, $Re = 1$, $\Lambda = 0$, and $W = 0.1$: (a) Velocity; (b) Stress. Initial profiles in black; profiles at intervals $Dt = 0.0158$ (blue) and $Dt = 0.00158$ (red).

flow.

The convergence of the mean velocity for the two cases is shown in Fig. 17. The main noticeable difference is for $W = 0.1$ where the convergence is monotone. Compared to the earlier stopping flow, the steady profile is now non-zero, hence the fluidity does not vanish and damping of the transient is more effective. This is also true for $W = 10$,

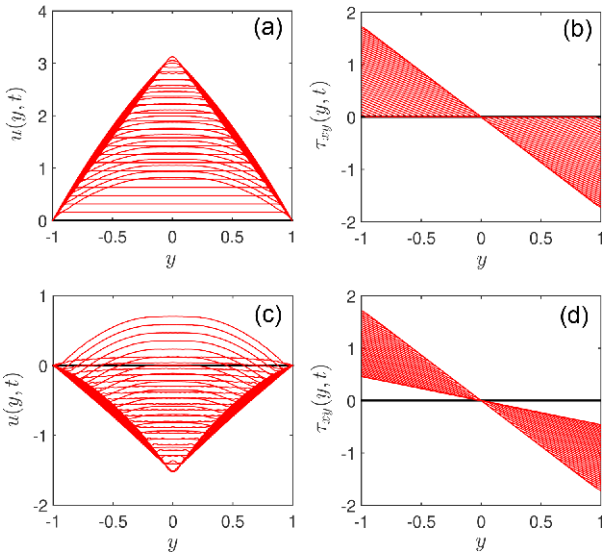

Fig. 16. (Color online) Startup flow for non-thixotropic BMP fluid with $Y = 0.25$, $Re = 1$, $\Lambda = 0$, and $W = 10$: (a) and (c) velocity; (b) and (d) stress. Figures (a) and (b) $t \in [0, 2\sqrt{ReW}]$; figures (c) and (d) $t \in [2\sqrt{ReW}, 4\sqrt{ReW}]$.

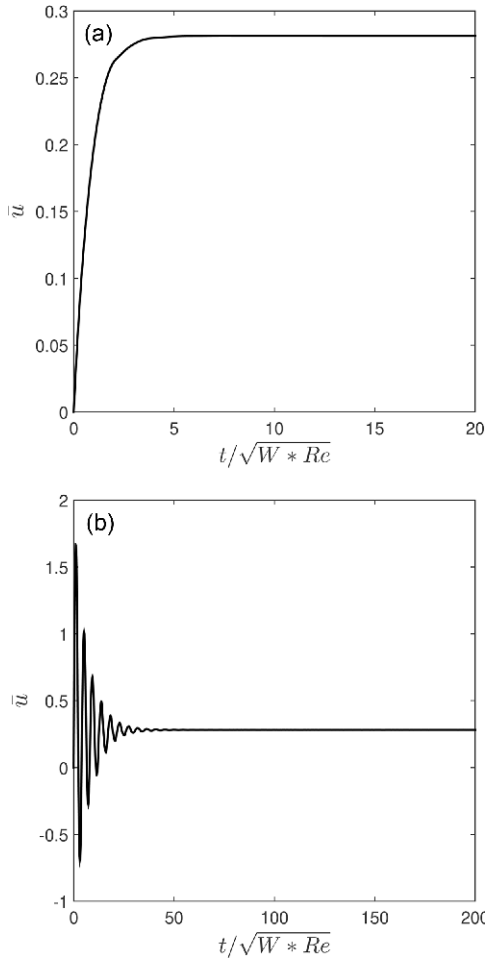

Fig. 17. Variations in mean velocity with time for: (a) Fig. 15; (b) Fig. 16.

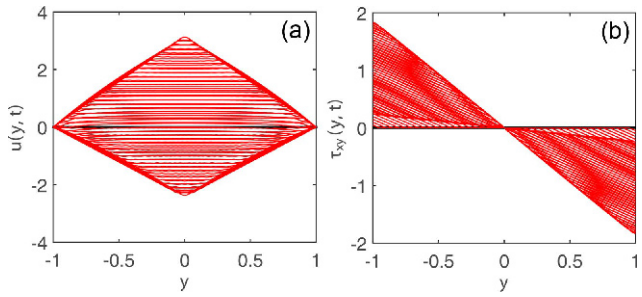

Fig. 18. (Color online) Startup flow for non-thixotropic BMP fluid with $Y = 1.5$, $Re = 1$, $\Lambda = 0$, and $W = 10$: (a) Velocity; (b) Stress. Initial profiles in black; profiles at intervals $Dt = 0.158$.

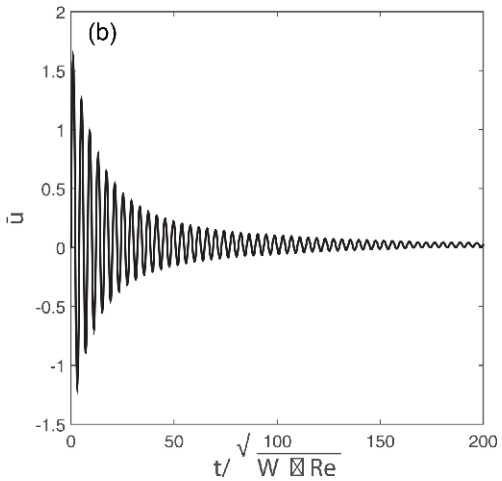

Fig. 19. Variation in mean velocity for flow of Fig. 18.

except less visible since the initial elastic oscillations are much more significant. However, comparing Fig. 17b with Fig. 14b the convergence is faster for the non-zero steady flow.

Lastly, we consider the same elastic restart of Fig. 16, except now with $Y = 1.5$. The flow again restarts with a large elastic oscillation in both velocity and stress; see Fig. 18. However, now $Y > Y_c = 1$ and the underlying steady Poiseuille flow is $u = 0$. Thus, the restart is short lived and the flow eventually decays to zero.

Comparing decay of the mean velocity in Fig. 18 to that of Fig. 16, the decay is significantly slower; see Fig. 19. This is slightly paradoxical if we think of Y as the yield stress, which for simple yield stress fluid models viscosifies. Here increasing Y makes the fluid more gel-like, suppressing the mean fluidity which suppresses the effect of damping.

6. Conclusions

In this short paper we have studied the various limits of the classical BMP model when eliminating either elasticity or thixotropy. The aim has been to study how the energy stability of the underlying visco-plastic system (for $\hat{\varphi}_0 = 0$) is affected. The key results are that for the VP system with $\Lambda = W = 0$ the flow behaves qualitatively as does any simple yield stress fluid, *e.g.*, Bingham, Casson etc.. The main point is that the dissipation $\langle \underline{\underline{\boldsymbol{\tau}}} : \dot{\underline{\underline{\boldsymbol{\gamma}}}} \rangle$, evaluated for the steady kinetic and constitutive models should increase monotonically with the strain rate and approach zero linearly, when expressed as a function of the strain rate. Loss of the monotonicity might not affect critical yield number behaviour, but would affect uniqueness of steady solutions and potentially the stability, *e.g.*, shear-banding.

Thus, this analysis gives some general guidelines for the construction of constitutive models that preserve features of yield stress behaviour with respect to static stability. In fact there is considerable flexibility in how such models could be constructed while retaining this behaviour. For example, the steady kinetic equation could be varied, or the stress could be split into solvent and polymeric parts, or adapted to model suspensions as with Calderas *et al.* (2013). Alternately, when splitting into solvent and polymeric parts, one might consider to include the yield stress behaviour directly as part of the solvent stress. Mathematically, this makes little difference within the BMP framework insofar as VP flows are concerned. Additionally, we remark that our focus on the BMP model is somewhat arbitrary. Others have developed kinetic models that have a stronger focus on rheological aspects of yielding, *e.g.*, Leonov (1990), and there are many other thixotropy models included in the reviews of Mujumdar *et al.* (2002), Mewis and Wagner (2009), that deserve more analysis.

The BMP model of Bautista *et al.* (1999) was a straightforward elastic extension of the earlier model of Fredrickson (1970). In many studies since the flows considered have been viscometric, for which the precise format of the model is not particularly important since φ remains bounded. However, for more complex flows this is not the case, due to the dissipation term. It is only in more recent computational studies such as López-Aguillar *et al.* (2018) that the positivity of the dissipation has been fixed by using $|\underline{\underline{\boldsymbol{\tau}}} : \dot{\underline{\underline{\boldsymbol{\gamma}}}}|$, which keeps the fluidity bounded.

An alternative to this treatment is to replace the dissipation with *e.g.*, $\varphi\tau^2$ or $\dot{\gamma}^2/\varphi$. Either option would ensure positivity and produce the same results for 1D steady flows. Consideration of kinetic equations that model destruction via either strain rate or stress is discussed by de Souza Mendes and Thompson (2012), who advocate use of the stress. We agree entirely with this. As well as the physical arguments raised by de Souza Mendes and Thompson, we see that using the stress in the kinetic equation here gives a much clearer interpretation of Y. For example, for the EVP flows we have $\varphi = \varphi_s(\tau/Y)$ so that $\tau \leq Y$ implies directly that $\varphi = 0$. For TVP flows we have the same physical interpretation of Y as a threshold value

for the steady fluidity. This does not affect critical Y for either system and stability results appear the same for the TVP flows.

A last remark concerns the EVP flows, which we have seen can exhibit significant elastic waves in some of our simple examples. The disappearance of damping in the model is a bit peculiar. This could be rectified by splitting the stress into a solvent and polymer part, *i.e.*, retaining viscous damping, or by looking at non-vanishing $\hat{\varphi}_0$. There are also many other ways in which to make the underlying Fredrickson model elastic. A number of such methods have already been considered within the BMP framework in the literature for either analytical, experimental or computational reasons, *e.g.*, Tabatabaei *et al.* (2015). Whether elastic modelling can be considered separately from the yield stress behaviour remains unclear and depends on the origin of the yield stress in the system under investigation.

Acknowledgement

This paper has been written to commemorate the 30th anniversary of the Korean Society of Rheology in 2019. We wish the KSR many more years of successful scientific endeavor and are grateful to them for providing the impetus to look into the BMP model, itself 20 years old in 2019. The research has been carried out at the University of British Columbia, supported by Natural Sciences and Engineering Research Council of Canada via their Discovery Grants programme (Grant No. RGPIN-2015-06398). The authors also express their gratitude to the Mexican National Council for Science and Technology (SENER-CONACYT) for financial support (AR).

References

Balmforth, N.J., I.A. Frigaard, and G. Ovarlez, 2014, Yielding to stress: Recent developments in viscoplastic fluid mechanics, *Annu. Rev. Fluid Mech.* **46**, 121-146.

Bautista, F., J. de Santos, J.E. Puig, and O. Manero, 1999, Understanding thixotropic and antithixotropic behavior of viscoelastic micellar solutions and liquid crystalline dispersions. I. The model, *J. Non-Newton. Fluid Mech.* **80**, 93-113.

Bautista, F., J.H. Pérez-López, J.P. Garcia, J. Puig, and O. Manero, 2007, Stability analysis of shear banding flow with the BMP model, *J. Non-Newton. Fluid Mech.* **144**, 160-169.

Boek, E.S., J.T. Padding, V.J. Anderson, P.M.J. Tardy, J.P. Crawshaw, and J.R.A. Pearson, 2005, Constitutive equations for extensional flow of wormlike micelles: Stability analysis of the Bautista-Manero model, *J. Non-Newton. Fluid Mech.* **126**, 39-46.

Bonn, D., M.M. Denn, L. Berthier, T. Divoux, and S. Manneville, 2017, Yield stress materials in soft condensed matter, *Rev. Mod. Phys.* **89**, 035005.

Calderas, F., E.E. Herrera-Valencia, A. Sanchez-Solis, O. Manero, L. Medina-Torres, A. Renteria, and G. Sanchez-Olivares, 2013, On the yield stress of complex materials, *Korea-Aust. Rheol. J.* **25**, 233-242.

Castillo, H.A. and H.J. Wilson, 2018, Elastic instabilities in pressure-driven channel flow of thixotropic-viscoelasto-plastic fluids, *J. Non-Newton. Fluid Mech.* **261**, 10-24.

Coussot, P., Q.D. Nguyen, H.T. Huynh, and D. Bonn, 2002, Viscosity bifurcation in thixotropic, yielding fluids, *J. Rheol.* **46**, 573-589.

de Souza Mendes, P.R., B. Abedi, and R.L. Thompson, 2018, Constructing a thixotropy model from rheological experiments, *J. Non-Newton. Fluid Mech.* **261**, 1-8.

de Souza Mendes, P.R. and R.L. Thompson, 2012, A critical overview of elasto-viscoplastic thixotropic modeling, *J. Non-Newton. Fluid Mech.* **187**, 8-15.

de Souza Mendes, P.R. and R.L. Thompson, 2019, Time-dependent yield stress materials, *Curr. Opin. Colloid Interface Sci.* **43**, 15-25.

Dimitriou, C.J. and G.H. McKinley, 2019, A canonical framework for modeling elasto-viscoplasticity in complex fluids, *J. Non-Newton. Fluid Mech.* **265**, 116-132.

Duvaut, G. and J.L. Lions, 1976, *Inequalities in Mechanical and Physics*, Springer, New York.

Ewoldt, R.H. and G. McKinley, 2017, Mapping thixo-elasto-visco-plastic behavior, *Rheol. Acta* **56**, 195-210.

Fraggedakis, D., Y. Dimakopoulos, and J. Tsamopoulos, 2016, Yielding the yield stress analysis: A thorough comparison of recently proposed elasto-visco-plastic (EVP) fluid models, *J. Non-Newton. Fluid Mech.* **236** 104-122.

Fredrickson, A.G., 1970, A model for the thixotropy of suspensions, *AIChE J.* **16**, 436-441.

Frigaard, I., 2019a, Simple yield stress fluids, *Curr. Opin. Colloid Interface Sci.* **43**, 80-93.

Frigaard, I.A., 2019b, Background Lectures on Ideal Visco-Plastic Fluid Flows, In: Ovarlez, G. and S. Hormozi, eds., *Lectures on Visco-plastic Fluid Mechanics*, Springer International Publishing, 1-40.

Holenberg, Y., O.M. Lavrenteva, U. Shavit, and A. Nir, 2012, Particle tracking velocimetry and particle image velocimetry study of the slow motion of rough and smooth solid spheres in a yield-stress fluid, *Phys. Rev. E* **86**, 066301.

Karimfazli, I. and I.A. Frigaard, 2016, Flow, onset and stability: Qualitative analysis of yield stress fluid flow in enclosures, *J. Non-Newton. Fluid Mech.* **238**, 224-232.

Leonov, A.I., 1990, On the rheology of filled polymers, *J. Rheol.* **34**, 1039-1068.

López-Aguilar, J.E., M.F. Webster, H.R. Tamaddon-Jahromi, and O. Manero, 2018, Predictions for circular contraction-expansion flows with viscoelastoplastic and thixotropic fluids, *J. Non-Newton. Fluid Mech.* **261**, 188-210.

Manero, O., F. Bautista, J.F.A. Soltera, and J.E. Puig, 2002, Dynamics of worm-like micelles: The Cox-Merz rule, *J. Non-Newton. Fluid Mech.* **106**, 1-15.

Mewis, J. and N.J. Wagner, 2009, Thixotropy, *Adv. Colloid Interface Sci.* **147**, 214-227.

Moller, P., A. Fall, V. Chikkadi, D. Derks, and D. Bonn, 2009, An attempt to categorize yield stress fluid behaviour, *Phil. Trans.*

R. Soc. A-Math. Phys. Eng. **367**, 5139-5155.
Mujumdar, A., A.N. Beris, and A.B. Metzner, 2002, Transient phenomena in thixotropic systems, *J. Non-Newton. Fluid Mech.* **102**, 157-178.
Oldroyd, J.G., 1947, A rational formulation of the equations of plastic flow for a Bingham solid, *Math. Proc. Camb. Philos. Soc.* **43**, 100-105.
Putz, A.M.V., T.I. Burghelea, I.A. Frigaard, and D.M. Martinez, 2008, Settling of an isolated spherical particle in a yield stress shear thinning fluid, *Phys. Fluids* **20**, 033102.
Saramito, P., 2007, A new constitutive equation for elastoviscoplastic fluid flows, *J. Non-Newton. Fluid Mech.* **145**, 1-14.
Saramito, P., 2009, A new elastoviscoplastic model based on the Herschel–Bulkley viscoplastic model, *J. Non-Newton. Fluid Mech.* **158**, 154-161.
Schwedoff, T., 1900, La rigidite des fluids, *Rapports du Congrés Intern. de Physique.* **1**, 478-486.
Tabatabaei, S., J.E. López-Aguilar, H.R. Tamaddon-Jahromi, M.F. Webster, and R. Williams, 2015, Modified Bautista-Manero (MBM) modelling for hyperbolic contraction-expansion flows, *Rheol. Acta* **54**, 869-885.